Novel Structural Changes During Temperature-Induced Self-Assembling and Gelation in Aqueous Solutions of the Copolymer $PLGA_{1170}$-PEG_n-$PLGA_{1170}$

Neda Khameh Khorshid

Supervisors

Prof. Bo Nyström

Prof. Sverre Arne Sande

Department of Chemistry

Faculty of Mathematics and Natural Sciences

University of Oslo

May 2013

Acknowledgement

One of the joys of completion in any task is to look over the journey passed and remember all the friends and family who have helped and supported me along this long but fulfilling road.

This master thesis could not have been done without the generous assistance and encouragement of many individuals.

In this regard, I would especially like to express my profound gratitude to my two supervisors Prof. Bo Nyström and Prof. Sverre Arne Sande without whom this project could not have been accomplished. I greatly value their encouragement, open-handedness in offering advice and availability for consultation. Many thanks to Prof. Kenneth Knudsen to give me the chance to have access to SANS instrument at IFE. I also thank Dr. Kaizheng Zhu for synthesizing the polymers which are studied in this thesis.

The two-year Master degree I took at University of Oslo (UiO) made it possible for me to find great worthy friends (Golnaz Isapour, Sara Bekhradnia, Elahe Jafari, Leva Momtazi, Farinaz Kahnamouei and Dr. Shahla Bagheri) that I will never forget. I wish to thank all, especially Dr. Atoosa Maleki, Dr. Reidar Lund and Erfan Dashtimoghadam for what I have learned from them.

I would not have passed through this road if it wasn't for my parents, who instilled in me passion for science, all of which finds a place in this thesis. To my parents, my brother and sister, thank you.

Last, but not least, to my amazing husband Amir for being with me through the good and bad times. Amir, I could never express how much I love and respect you for that.

Neda Khameh Khorshid

May 2013

Abstract

Effects of temperature on phase behavior and sol-gel transition in aqueous solutions of poly (D,L-lactide-co-glycolide-*b*–ethylene glycol-*b*-D,L-lactide-co-glycolide) (abbreviated as PLGA–PEG–PLGA) triblock copolymers with different PEG length (M_n=1000 and 1500 g/mol) were investigated by means of turbidimetry, dynamic light scattering (DLS), Rheo-small angle light scattering (Rheo-SALS), and small-angle neutron scattering (SANS) techniques. Chemical structure and composition of synthesized copolymers were also characterized by proton nuclear magnetic resonance (^{1}H NMR) Spectroscopy.

The association properties of PLGA-PEG_{1000}-PLGA and PLGA-PEG_{1500}-PLGA have been investigated at constant concentration (1.0 wt%). The results of turbidity showed that with increasing temperature association of chains occurs, while and at sufficiently high temperature the macroscopic phase separation is observed. The maximum of the turbidity was found to be at 30°C for PLGA-PEG_{1000}-PLGA and at 40°C for PLGA-PEG_{1500}-PLGA. It was realized the longer PEG length induces elevated cloud point (CP) temperature and a decrease of turbidity at high temperatures in dilute aqueous copolymer solution (1.0 wt%). SANS measurements revealed that the copolymer PLGA-PEG_{1000}-PLGA creates very large extended plates upon increasing temperature, which easily aggregate and sediment. This behavior is very different from the PLGA-PEG_{1500}-PLGA solution, which forms spherical micelles that are stable in the corresponding temperature range.

The temperature-induced gel formation of the amphiphilic triblock copolymers in semidilute regime (20 wt%) was studied. The triblock copolymers exhibited a reversible sol–gel transition in phosphate buffer (pH= 7.4). The phase diagram of the copolymers, concentration and temperature at which the solution no longer flows, was obtained by the “test tube inverting method”. These results suggest that the gelation temperature of the copolymer solutions can be influenced by their hydrophilicity.

The turbidity and rheology features of the PLGA-PEG_{1000}-PLGA and PLGA-PEG_{1500}-PLGA as well as their mixture versus temperature at a total polymer concentration of 20 wt% have been studied. The turbidity results disclosed that the interchain aggregations are more pronounced for the pure PLGA-PEG_{1000}-PLGA with total concentration of 20 wt%, and a new transition peak in the turbidity curve was observed. The first turbidity peak was appeared at 20°C and then turbidity dropped at 30°C. A new turbidity peak appeared above 30°C and finally a minor change was seen between 40°C and 50°C. Oscillatory rheometric measurements were employed to determine the gel point and also quantify the viscoelastic features of the physical copolymeric gels. It has been shown that the gel window could be tuned by the PEG block length. Moreover, the shorter PEG block found to have more subtle effect on the sol-gel transition temperature, storage modulus, and viscosity of the resulting hydrogels. The lowest gelation temperature was observed in the case of pure PLGA-PEG_{1000}-PLGA, while increasing PLGA-PEG_{1500}-PLGA composition in the mixture solutions resulted in elevated gel points. Based on the Winter and Chambon theory,

a similar power law frequency dependence of the dynamic storage modulus ($G' \propto \omega^{n'}$) and loss modulus ($G'' \propto \omega^{n''}$) is observed at the gel point $n' = n'' = n$. Viscoelastic exponent of ($n = 0.53$) was obtained for PLGA-PEG$_{1000}$-PLGA, and accordingly the critical gel strength parameter of ($S = 16$) and the fractal dimension of ($d_f = 1.96$) was calculated. In this regard, it was found that with increasing the content of PLGA-PEG$_{1500}$-PLGA in the blend gels, looser networks with open structure at higher temperature are formed. The SANS patterns exhibited a strong change at different temperatures, which indicates change in the micellar structures. The distinct peak for PLGA-PEG$_{1000}$-PLGA at around $q = 0.03\ \text{Å}^{-1}$ implies a significant interaction between the micelles (20°C). With increasing temperature the peak transferred to higher *q* values and the size of the micelles is slightly reduced together with the disappearance of the correlation peak. The shape of curve is very different from the other temperatures at 30°C. It seems that the self-assembled structure changes from spherical micelle to cylinder micelles and at the higher temperature (40 - 50°C) into hexagonal micelles.

Overall, the obtained results converge to indicate that the developed copolymeric gels with customized gelation temperature, microstructure and stiffness could be considered as injectable carries for various biomedical applications, such as controlled drug delivery systems and tissue engineering.

Persian Abstract

چکیده

کوپلیمر PLGA-PEG-PLGA با طولهای مختلف (M_n=1000,1500) PEG با استفاده ازکدری سنجی [1],تفرق کم زاویه نوترونی [2] و رئولوژی [3] مورد بررسی قرار گرفته است . ساختار و ترکیب شیمیایی کوپلیمر ساخته شده بوسلیه ^{1}HNMR شناسایی شده است .

نتایج حاصل ازکدری سنجی در حالت رقیق نشان میدهد با افزایش دما، موجب تجمع زنجیره‌های کوپلیمر 4PLGA-PEG-PLGA میشود. در حالی که در دماهای بالاتر جدایی فاز رخ داده است. با افزایش طول زنجیر PEG نقطه ابری (CP) افزایش و از کدری آن کاسته میشود.

نتایج SANS نشان میدهد ،کوپلیمر PLGA-PEG-PLGA با زنجیره PEG کوتاه تر، صفحه های پهن در دماهای بالا تولید میکند؛ در صورتیکه کوپلیمر با PEG بلندتر، میسلهای کروی رادر این محدوده دما تشکیل میدهند . تشکیل ژل از آمفیفیلیک در منطقه شبه رقیق توسط رئولوژی مطالعه شده است. این کوپلیمرها گذار از حالت محلول به ژل را در محیط بافر فسفات نشان میدهند. غلظت و دمایی که در آن محلول دیگر جاری نیست بوسلیه روش "لوله کج" بررسی شده. نتایج نشان میدهد کوپلیمرها میتوانند تحت تاثیر گروه‌های آبدوست خودشان باشند.

روشهای کدرسنجی و رئولوژی برای کوپلیمرها با غلظت ٪ wt ۲۰ نشان میدهند، کدورت نمونه که شامل PEG کوتاه تری است، قوی تر می‌باشد. با رئولوژی نقطه ژل را میتوان اندازه گیری کرد. که نشان میدهد اندازی زنجیر PEG بر روی ساختار ژل تاثیر میگذرد . نتایج بدست آماده از SANS و تغییر شکل گرافها، حاکی از آن است که در دماهای مختلف شکل میسلها از حالت کروی به حالت استوانه ای تغییر مییابد .

به طور کلی نتایج بدست آمده نشان میدهد، این کوپلیمرها میتوانند در زمینه های پزشکی مثل حاملهای دارو و مهندسی بافت بکار روند .

---

1. Turbidimetry
2. Small Angle Neutron Scattering (SANS)
3. Rheology
4. Poly (D,L-lactic-co-glycolic-*b*–ethylene glycol-*b*-D,L-lactic-co-glycolic)

Table of Contents

ACKNOWLEDGEMENT 3

ABSTRACT 5

1. INTRODUCTION 16

2. THEORY AND BACKGROUND 18

2.1. Copolymers and Their Architectures 18

2.2. Amphiphilic Block Copolymer 19
2.2.1. Micellization 20
2.2.2. Gelation 23

2.3. Hydrogels 23
2.3.1. Stimuli-Sensitive Block Copolymer Hydrogels 24
2.3.2. Temperature-Sensitive Block Copolymer Hydrogels 24

2.4. Gel point 27

2.5. Synthesis of Block Copolymers 27

2.6. Amphiphilic Block Copolymer Applications 28

2.7. PLGA Properties 28

2.8. PEG Properties 29

2.9. PLGA-PEG-PLGA Properties 30

2.10. Pluronic and PLGA-PEG-PLGA 31

2.11. Block Copolymer Characterization Methods 32
2.11.1. Test Tube Inverting Method 33
2.11.2. Turbidimetry 33
2.11.3. Rheology 35
2.11.3.1. Oscillatory Shear Measurements 37
2.11.3.2. Determination of the Gel Point 39
2.11.3.3. Gel Strength Parameter 40
2.11.3.1.1. Theoretical Models for the Interpretation of n 40
2.11.4. Rheo-Small Angle Light Scattering (rheo-SALS) 42
2.11.5. Small Angle Neutron Scattering 44
2.11.5.1. Core – Shell Micelles 46

3. EXPERIMENTAL SECTION 48

3.1. Materials 49

3.2. Synthesis **49**

3.3. Sample Preparation **52**

3.4. Test Tube Inverting Method **53**

3.5. Turbidimetry **53**

3.6. Small Angle Neutron Scattering **54**

3.7. Rheometer **55**

3.8. Rheo-SALS **56**

4. RESULTS AND DISCUSSION **56**

4.1. Dilute Solutions **56**
4.1.1. Turbidimetry 56
4.1.2. Small Angle Neutron Scattering 58

4.2. Semidilute Solutions **61**
4.2.1. Test Tube Inverting Method 61
4.2.2. Turbidimetry 63
4.2.3. Rheology 67
4.2.3.1. Determination of Gel Point 67
4.2.4. Rheo-Small Angle Light Scattering (rheo-SALS) 71
4.2.5. Small Angle Neutron Scattering (SANS) 74

5. CONCLUSION **80**

6. REFERENCE **84**

List of Symbols and Abbreviations

ATRP	Atom Transfer Radical Polymerization
CAC	Critical Aggregation Concentration
CGC	Critical Concentration of Gelation
CGT	Critical Gel Temperature
CLRP	Controlled Living Radical Polymerization
CMC	Critical Micelle Concentration
CMT	Critical Micelle Temperature
CP	Cloud Point
Cryo-TEM	Cryogenic Temperature Transmission Electron Microscopy
D_c	Cooperation Diffusion Coefficient
DLS	Dynamic Light Scattering
d	Space Dimension
d_f	Fractal Dimension
eq.	Equation
FDA	Food and Drug Administration
G(t)	Relaxation Modulus
G'(ω)	Storage Modulus
G"(ω)	Loss Modulus
GA	Glycolic Acid

GP	Gel Point
GPC	Gel Permeation Chromatography
I(q)	Scattering Intensity
I_t	Transmitted Light Intensity
I_0	Incident Light Scattering
j_1	Standard Mathematical Function
L	Path Length of the Light in the Cuvette
LA	Lactic Acid
LCST	Lower Critical Solution Temperature
M	Mass of a Molecular Cluster
M_n	Number Average Molecular Weight
n	Relaxation Exponent
n'	Power Law Parameter ($G' \sim \omega^{n'}$)
n''	Power Law Parameter ($G'' \sim \omega^{n''}$)
n_p	Number Density of Particles
P(q)	Form Factor
P	Bond Probability (a Measure of Connectivity)
P_c	Critical Extent of Reaction
PEG	Polyethylene glycol
PEO–PPO–PEO	Pluronic

PEO	Poly (ethylene oxide)
PLGA	Poly (lactic-co-glycolic acid)
PPO	Poly (propylene oxide)
q	Wave Vector
R_g	Radius of Gyration
R_h	Hydrodynamic Radius
RAFT	Reversible Addition-Fragmentation Chain Transfer
Rheo-SALS	Rheo-Small Angle Light Scattering
ROP	Ring Opening Polymerization
r	Scaling Exponent
r_c	Radius of Core
S	Gel Strength Parameter
S(q)	Structure Factor
SANS	Small Angle Neutron Scattering
SAXS	Small Angle X-ray Scattering
SLS	Static Light Scattering
$Sn(Oct)_2$	Stannous Octoate
T	Temperature
T_{gel}	Gel Temperature
T_{turbid}	Turbidity Temperature

$T_{precipitation}$	Precipitation Temperature
TMS	Tetra Methyl Silane
t	Thickness of Shell
tan δ	Damping factor or Loss Tangent
UCST	Upper Critical Solution Temperature
V_C	Volumes of Core
V_S	Volumes of Shell
wt %	Weight Percentage
α	Power Law Index ($\eta\ \dot{\gamma}^{(\alpha-1)}$)
Γ	Legendre Gamma Function
γ	Strain
$\dot{\gamma}$	Shear rate
γ_0	Maximum Amplitude for Strain
ΔG	Gibbs Free Energy
ΔH	Enthalpy Change
ΔS	Entropy Change
δ	Phase Angle
δ_{cs}	Chemical Shift
η	Viscosity
θ	Scattering Angle

θ_0	Gap Angle
λ	Wavelength
ν	Frequency
ξ_D	Dynamic Correlation Length
ξ_S	Static Correlation Length
ρ_v	Scattering Length Density of Core
ρ_s	Scattering Length Density of Shell
ρ_{solv}	Scattering Length Density of Solvent
$d\Sigma/d\Omega$	Coherent Differential Cross Section
σ_0	Maximum Amplitude Stress
τ	Turbidity
ω	Angular Frequency (rad/s)

1. Introduction

Self-aggregation of amphiphilic block copolymers in aqueous media and their sol-to-gel transition are of special interest for various applications [1]. These copolymers are considered as smart systems, which are able to respond to environmental stimulus including chemical substances, temperature, pH, electric field, etc [2].

Over the past decade, thermosensitive copolymers have become increasingly attractive as injectable carriers for delivery of biological as well as pharmaceutical agents [3]. While the core of block copolymer micelles can load hydrophobic drugs, the hydrophilic blocks form a shell around the micelles due to hydrogen bonds with the aqueous surroundings. Protein adsorption and cellular adhesion are prevented by micelles with a corona and the hydrophobic core supports drug against hydrolysis and enzymatic degradation. The micelles are not recognized with reticuloendothelial because of the corona, so it allows drugs to be distributed and circulated over a long time. A final feature that makes amphiphilic block copolymers attractive for drug delivery applications is the fact that their chemical composition, total molecular weight, and block length ratios can be easily changed, which allows to control over the size and morphology of the micelles [4].

In dilute regime, PLGA-PEG-PLGA self-assembles in aqueous solution and exists in form of micelles. Various types of micelles could be formed in aqueous media depending on the structure of block chains in copolymer. The copolymer with longer PEG length induces a flower-type micellar shape, in which the middle PEG

chain makes a loop on the surface. It is possible that the copolymer with shorter PEG length does not form the flower-like micelle [5]. Due to the difference in shape of micellar structures from PLGA-PEG-PLGA to other copolymers, it is interesting to compare the structurally different triblock copolymers in terms of their effect on various applications [6]. A class of triblock copolymers (Pluronics or Poloxamers) composed of poly (ethylene glycol-b-propylene glycol-b-ethylene glycol) show a reversible sol-gel transition by a small pH and temperature change [3, 7]. Poloxamer 407 hydrogels have been used as drug delivery systems for external application of anticancer drugs, burn treatments, anti inflammatory drugs, antibiotics tridecapeptide, melanotan-I (MT-I), mitomycin C, interleukin-2 and urease. Poloxamer 407 hydrogels have also employed for a sustained release of human growth hormone (rhGH) in vitro for 60 –72 h and for a week in vivo following intramuscular and subcutaneous injections [8]. However, Poloxamers are not considered as optimal system for the delivery of protein drugs because they are not biodegradable and show toxicity at the high concentration (>16 w/w %). Therefore, new injectable biodegradable polymers such as PLGA-PEG-PLGA have been studied as controlled release drug carriers, owing to their nontoxicity and biocompatibility. They are forming depots that slowly degrade over a period of 4–6 weeks [3]. PLGA-PEG-PLGA is a copolymer that undergoes phase separation in aqueous solution at elevated temperatures. Phase separation temperature in aqueous solution of the copolymer is investigated by using inverted test-tube method [5]. The core-shell micellar structure with longer hydrophobic chain length induces a weaker intermolecular association [9].

The aim of this study is to gain a deeper insight how the change in length of hydrophilic segment affects the structural characteristics, rheological features and dynamics of triblock copolymeric chains. In this study, we tried to investigate the self-aggregation behavior of PLGA-PEG-PLGA chains with different PEG length at different temperatures.

2. Theory and Background

2.1. Copolymers and Their Architectures

The main feature of a polymer is determined by its component monomers. The polymer structure has an important effect on determining physical properties of the macromolecular chains. Polymers that consist of identical monomers are known as homopolymers, whereas polymers consist a blend of monomers are known as copolymers linked by covalent bonds. The size and the length of chains within the polymer have an excrement effect on phase behavior, size of the micelles in solutions, viscosity and mobility of chains in solution. Generally, with increasing the chain length, chain interactions like van der Waals attractions increase.

Monomer arrangement in copolymers form a variety of architectures, including random, alternating, blocks and grafted copolymers (Figure 2.1) [10]. A three-step reaction enables preparation of (ABA) or (BAB) copolymers [11].

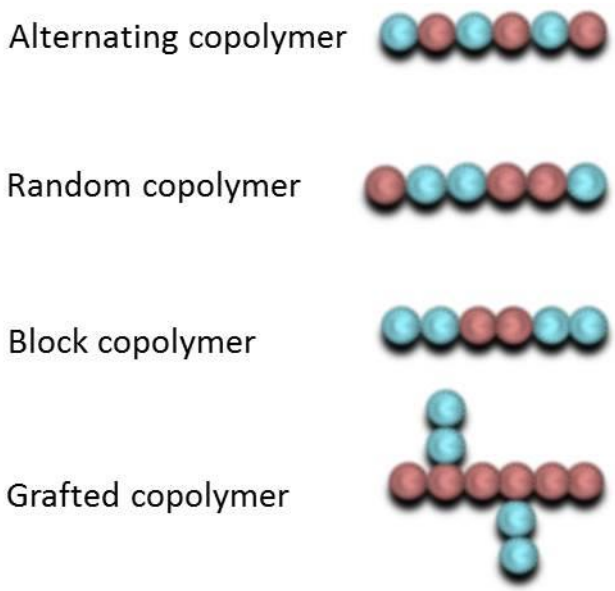

Figure 2.1 Different architectures of AB copolymers.

As mentioned above, block copolymers are composed of blocks of different polymerized monomers joined to each other. When two or three blocks with two different chemical types are joined within a polymer chain are called diblock or triblock copolymer, respectively, and if the three blocks have each of a different chemical types are called triblock terpolymers [12, 13].

2.2. Amphiphilic Block Copolymer

Amphiphilic polymers consist of at least two parts with different chemical nature including hydrophilic and hydrophobic blocks [14]. Amphiphilic is a Greek compound word of the “amphi” both and “philic” attraction [15]. Amphiphiles with the molecular weight lower than 500 are called surfactant, and amphiphiles with the size 10-1000 times larger than the small ones are called large amphiphilic (diblock or triblock) [16].

Amphiphilic block copolymers undergo two basic processes in solvent media: micellization and gelation [15].

2.2.1. Micellization

Micellization occurs when a block copolymer is dissolved in a large amount of a selective solvent, which is thermodynamically favorable for one block and unfavored for the other [17]. Generally, the process of micelle formation of amphiphilic block copolymers in organic solvents is exothermic process, which the micelles form at high temperature. If the process takes place in aqueous solution, the micelles form at elevated temperature and the process is endothermic [18]. Micelles comprise a core with insoluble blocks which are surrounded with soluble and flexible blocks. The micelle shape is generally spherical but the shape can be changed with changing environment conditions. When the micellization takes place in dilute solutions of block copolymer at a certain temperature above a concentration, the concentration is called critical micelle concentration (CMC) or critical association concentration for polymeric micelles (CAC) [15, 19]. The thermosensitive copolymers evolve micelles at a certain temperature called critical micelle temperature (CMT) [18]. In aqueous solutions of amphiphilic triblock copolymers, the lengths of the hydrophobic and hydrophilic blocks affect the micellar structures, CMC and CMT. Diblock copolymers with long hydrophilic chains form micellar aggregates due to the highly positive curvature of the interface. The curvature decreases as the length of the insoluble block increases and a transition to rod-like micelles is perceived. If the length of the

insoluble block increases further then lamellar phases are favored. Depending on the concentration, stacked lamella or vesicular structures can be formed (Figure 2.2).

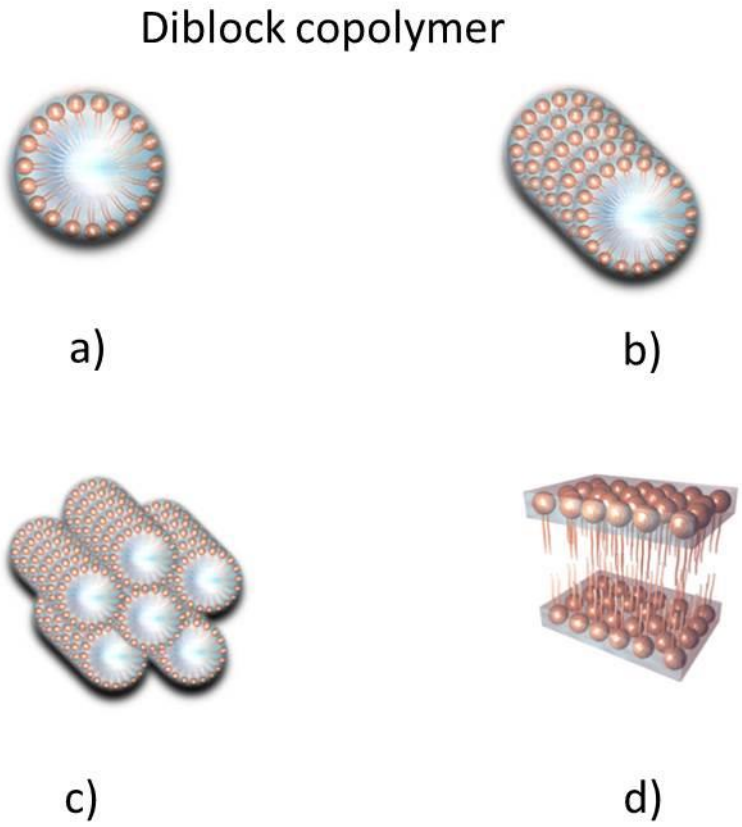

Figure 2.2 schematic representations of some of the different aggregation morphologies found in low molecular amphiphiles: a) spherical micelles; b) rod-like micelles; c) normal cylindrical hexagonal packing; d) lamella micelles.

In the case of triblocks comprising hydrophobic middle block, normal micelles form, whereas for triblocks with hydrophobic side chains flower-like micelles are perceived (Figure 2.3). At different temperatures various shapes of micelles like spherical, cylindrical and cylindrical hexagonal packing could be observed. Since this project is focused on amphiphilic triblock copolymers, more attention is paid on this type of polymers in the following.

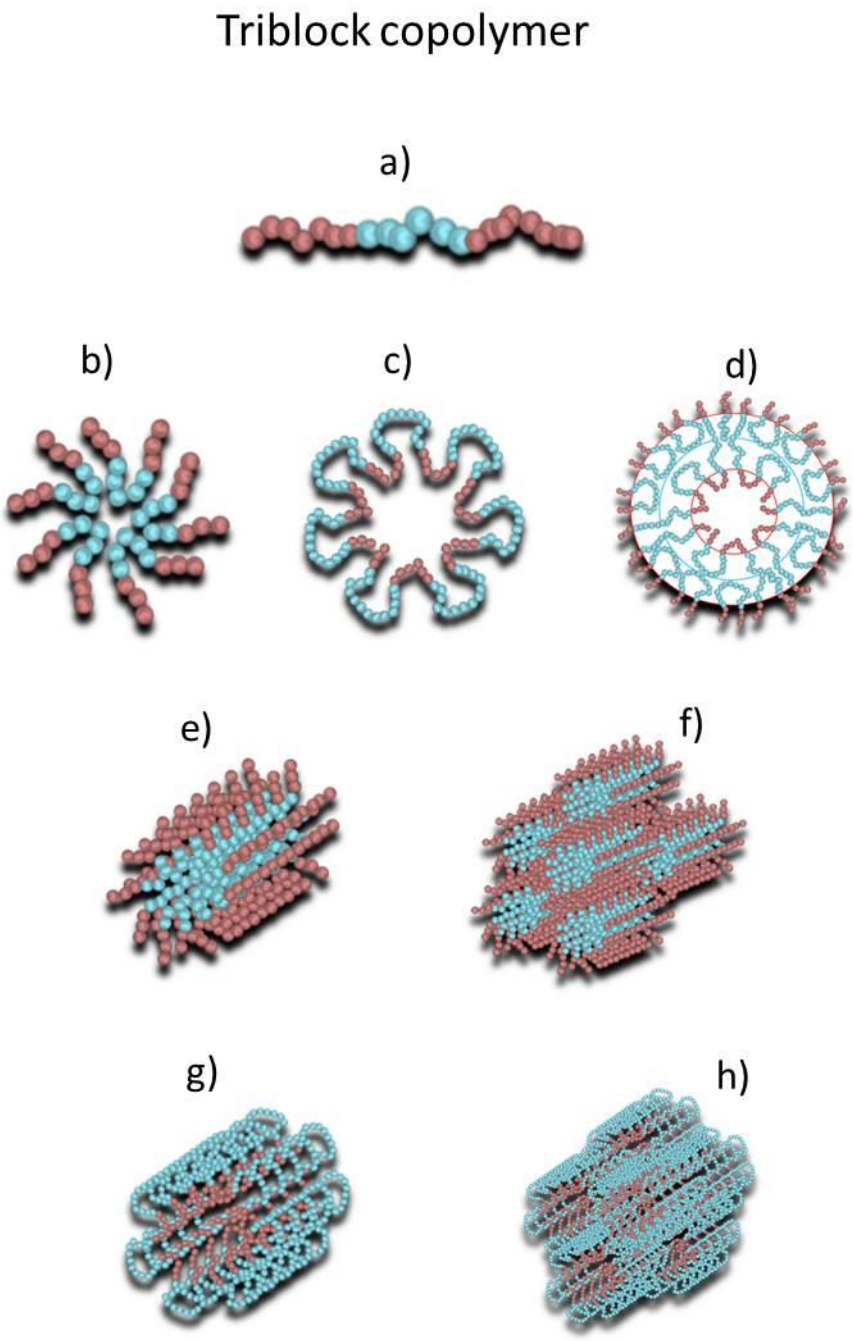

Figure 2.3 Schematic representation of: a) unimers in solution, triblock respectively b) normal c) flower-like micelles for a symmetric triblock-copolymer, d) vesicle formation for a triblock-copolymer respectively e) rod-like normal micelles f) normal cylindrical hexagonal packing g) rod-like flower-like micelles h) flower-like cylindrical hexagonal packing.

In contrast to micellization, gelation occurs from the semidilute to the high concentration regime of block copolymer solutions and results from an arrangement of ordered micelles [15].

2.2.2. Gelation

The problem of the transition of polymer solutions into gels (gelation) has always been considered as a classical subject of colloid chemistry. Gelation of a polymer solution can be characterized as a process involving a continuous increase in viscosity accompanied by a gradual enhancement of elastic properties. Gelation results in “freezing” of the whole system into a uniform non-flowing elastic mass. In this case it is resulting of the formation of a polymer structural network, encompasses the whole bulk of the system, and retains the solvent. The main cause of gelation in polymer systems is the enhancement of interactions between the dissolved polymer macromolecules or their aggregates. Gelation is usually related to poorer thermodynamic conditions and phase separation.

2.3. Hydrogels

Hydrogels are three-dimensional networks made of cross-linked hydrophilic or amphiphilic polymers that are swollen in liquid without dissolving in them [20]. Hydrogels are classified in smart materials, which have the capacity to absorb a large amount of water [21]. Hydrogels are used for biomedical applications such as drug or cell carriers and tissue engineering matrices [22]. These networks can be classified

into two main categories according to the type of cross-linking. The network cross-linked by covalent bonds form irreversible gels or chemical gels. In such gels, the number of tie-points essentially is not changed upon variation of the external conditions such as temperature, concentration or stress. In contrast, formation of a physical gel occurs via physical association of polymeric chains [23, 24].

2.3.1. Stimuli-Sensitive Block Copolymer Hydrogels

Stimuli-sensitive block copolymer hydrogels, are reversible polymer networks formed by physical interactions and exhibit a sol–gel phase transition [25]. Hydrogels can also control drug release by changing the gel structure in response to environmental stimuli like temperature and pH [26]. Simple drug formulation and administration procedures, less systemic toxicity and ability to deliver both hydrophilic and hydrophobic drugs are the advantages of environment- sensitive hydrogels [27]. In this project, temperature stimulus and its effect on the structure and size of micelles have been studied.

2.3.2. Temperature-Sensitive Block Copolymer Hydrogels

Temperature is one of the major parameters for stimuli-sensitive hydrogels, as it is easy to be controlled and has practical advantages both *in vitro* and *in vivo*. Thermoresponsive polymers have at least one block with a lower critical solution temperature (LCST) while another block represent an upper critical solution temperature (UCST), which the polymer chains are entirely soluble (Figure 2.4) [28].

A polymer solution below the LCST is transparent, while above the LCST, it emerges opaque. This phenomenon occurs because it is energetically more favorable. Applying Gibbs free energy equation $\Delta G = \Delta H - T\Delta S$, when the polymer is insoluble, the water is less arranged and has higher entropy that is the reason for phase separation known as “hydrophobic effect”. LCST is an entropically driven effect while UCST is an enthalpically driven effect [29]. With increasing temperature the LCST polymers represents a hydrophilic-to-hydrophobic transition, whereas the UCST systems indicates the opposite manner [30]. In most polymers, their solubility increases with increasing temperature, while in the case of polymers with LCST, solubility decreases as temperature increases due to dominating hydrophobicity interacts [31]. LCST is described as the temperature that polymer chains pass the phase transition from coil (soluble state) to globule (insoluble state) [32]. At low temperature, hydrogen bonding between the hydrophilic parts and the liquid is dominated, leading to more solubility in water. With increasing temperature, hydrophobicity increases and the stability of hydrogen bonding between the polymer and water decreases, so the hydrophobic interaction is dominated again. The LCST is observed at lower temperature for the polymer with more hydrophobicity. This property of thermosensitive polymers is made them attractive materials for injectable biomaterials, because of convenient mixing of polymer solution with drugs or therapeutic proteins at low temperature. At body temperature 37°C, a gel is formed *in situ*, containing the encapsulated drug in the network [33].

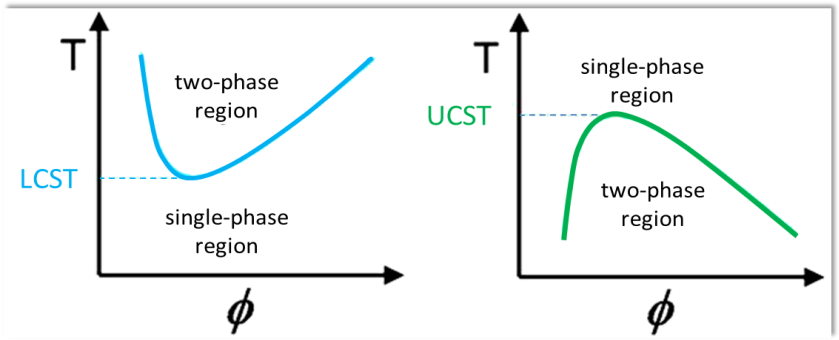

a) b)

Figure 2.4 Low critical solution temperature (LCST) and b) high critical solution temperature (UCST) in aqueous solution.

Triblock copolymers form micelles including a hydrophobic core and hydrophilic shell in aqueous solution at temperature below LCST. By raising the temperature above LCST these micelles aggregate and form the bridged micelles because of the hydrophobic interactions between the hydrophobic blocks (Figure 2.5).

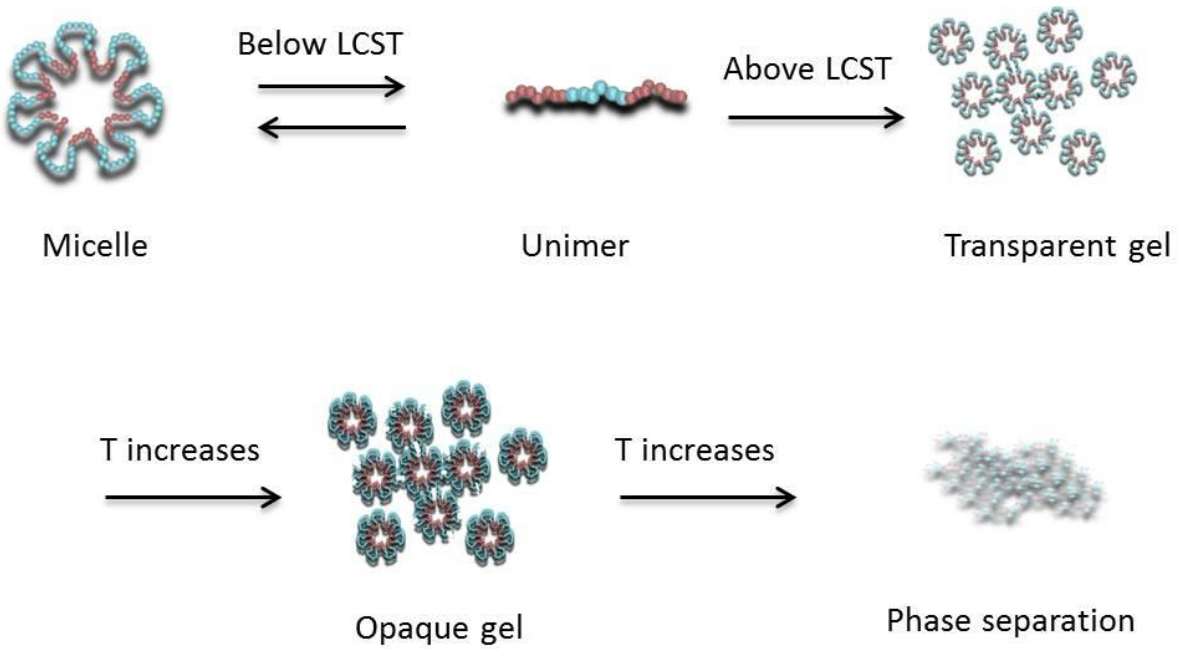

Figure 2.5 Triblock copolymers at different temperatures in aqueous solution.

2.4. Gel point

Gel point is a critical transition point, at which polymer shows liquid-like behavior before and solid-like behavior afterwards. Sol-gel transition is an example of percolation (P) that is determined by the emergence of macroscopic clusters. The gelation point is known as the critical point of percolation (P_C), which is determined by an incipient bond $(P \rightarrow P_C)$. In gel phase the sites are occupied more than critical value and form macroscopic network and small clusters $(P_C < P)$ hence, the solid polymer is not soluble even in a good solvent (only valid for chemically cross- linked gels). Below the critical level, clusters are available and the sol phase is obvious $(P < P_C)$. The critical concentration where the incipient gel forms is called critical gel concentration (CGC) [34]. The critical gelation temperature (CGT) forms the lower transition curve in the phase diagram [35]. Critical gel concentration and critical gel temperature will be discussed in this study based on composition of PEG-PLGA-PEG triblock copolymers and PEG block length.

2.5. Synthesis of Block Copolymers

Block copolymers are macromolecules consist of linear or nonlinear arrangements of chemically different polymeric blocks. Linear block copolymers are synthesized by different methods and some parameters like molecular weight, architecture and purity of the product has an important role to choose the method. General synthetic strategies for synthesis of block copolymers are anionic polymerization, cationic

polymerization, controlled radical polymerization, atom transfer radical polymerization (ATRP), reversible addition-fragmentation chain transfer radical polymerization (RAFT), controlled living radical polymerization (C/LRP) [19, 36]. Since the synthesis of block copolymers is not an addressed issue in this project, a detailed description of the synthesis methods has not been given, and this thesis is more focused on the characterization of the copolymers by various experimental methods.

2.6. Amphiphilic Block Copolymer Applications

Amphiphilic block copolymers have found applications in various fields due to their unique features, the ability to self-assembly and forming micelles [9]. They are usually used in medical and biomedical applications, especially in drug delivery and gene therapy [1, 37]. In literature, there are a number of applications in nanotechnology, reusable elastomeric materials, electronics [9], paints, cosmetics and lubricants and etc [15].

2.7. PLGA Properties

Poly (lactic-co-glycolic acid) (PLGA) is a copolymer with biodegradability and biocompatibility properties, which is approved by Food and Drug Administration (FDA) [38]. The random ring-opening co-polymerization is the method of synthesizing PLGA from their cyclic dimers of glycolic acid and lactic acid in the presence of catalyst stannous octane and chain control agent lauryl alcohol [39]. Synthetic polymers have the advantage of high purity and reproducibility over natural polymers [40]. By

changing the ratio of monomers, the polymer degradation and its properties are changed and this has made PLGA a good choice in the production of variety of biomedical devices such as grafts, sutures, implants, prosthetic devices, micro and nanoparticles[41]. PLGA is applied in nanomedicines because its hydrolysis and production of the main monomers, lactic acid and glycolic acid in the body[42].

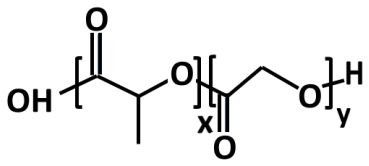

Figure 2.6 Structure of poly (lactic-co-glycolic acid), x= number of units of lactic acid; y= number of units of glycolic acid.

2.8. PEG Properties

Poly (ethylene glycol) (PEG) is polyester without interfering in the cellular functions. PEG is one of the most applied polymers in biomedical fields [43], which has been approved by FDA in different drug delivery systems (parenteral, topical, suppositories, nasal sprays), as well as foods and cosmetics applications [44]. PEG shows minimal systemic toxicity and high solubility in organic solvents and aqueous media compared to other hydrophilic polymers. Despite the fact that PEG has some impediments such as degradation under stress, hypersensitivity and toxicity of side products, it is still a high standard material for biomedical applications.

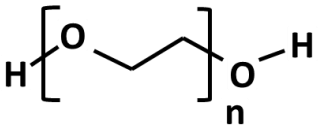

Figure 2.7 Schematic illustration of principal structure of PEG.

2.9. PLGA-PEG-PLGA Properties

Poly (D, L-lactic acid-co-glycolic acid)-*b*-poly (ethylene glycol)-*b*-poly (D, L-lactic acid-co-glycolic acid) (abbreviated as PLGA-PGE-PLGA) is a triblock copolymer including the hydrophobic and hydrophilic blocks [45]. This copolymer is dissolved in water owing to hydrophilicity of PEG and forms aggregates in high temperatures due to hydrophobic attractions between PLGA blocks [46]. The structure of the copolymer including the hydrophobic and hydrophilic blocks can be designed to modify the degradation rate, which plays an important role in controlled release applications. The properties like solubility in water and biodegradability have made PLGA-PGE-PLGA an interesting copolymer for drug delivery [3, 47].

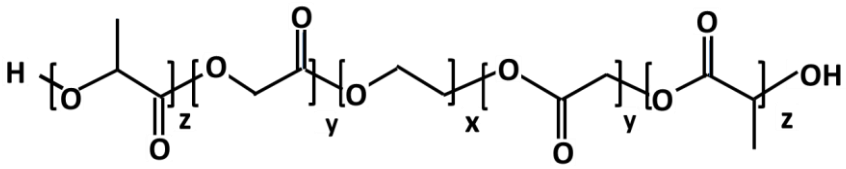

Figure 2.8 Schematic illustration of principal structure of PLGA-PEG-PLGA.

2.10. Pluronic and PLGA-PEG-PLGA

Poly (ethylene oxide)-poly (propylene oxide)-poly (ethylene oxide) (PEO–PPO–PEO) or Pluronic triblock copolymer solution is a free-flowing liquid at room temperature and it forms a gel at body temperature. The hydrophobic interaction is the reason for formation of self-associated micelles and gelation. The individual micelles are packed together and the rheological properties of copolymer changes above LCST [48]. Self-assembled Pluronic hydrogels which have shown low tissue-adhesion, low mechanical strength, rapid erosion, and fast drug release in vivo, are hardly applicable for tissue engineering and drug delivery purposes [49]. Therefore, new series of biodegradable triblock copolymers have been designed such as PLGA-PEG-PLGA. In contrast to Pluronic that has two hydrophilic PEO side segments and hydrophobic PPO segment in the middle, block PLGA-PEG-PLGA has a hydrophilic PEG middle segment and two hydrophobic PLGA segments in the side of chains [6]. Similarly, PLGA-PEG-PLGA shows a sol-gel transition behavior. The bridge micelles are formed in PLGA-PEG-PLGA solution, while the micellar packing (unimers to micelles) is observed in Pluronics. In spite of weaker gel network of Pluronics, PLGA-PEG-PLGA copolymers form stronger gels against erosion and the residence time of the gels increases.

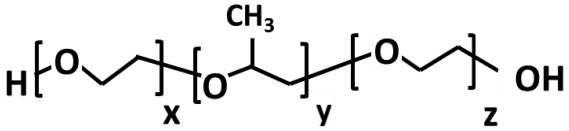

Figure 2.9 Schematic illustration of principal structure of PEO-PPO-PEO.

2.11. Block Copolymer Characterization Methods

Block copolymers are characterized by different methods. The structures of copolymers including weight average molecular (M_w) weight and number average molecular weight (M_n) are determined by gel permeation chromatography (GPC) and proton nuclear magnetic resonance spectroscopy (^{1}H NMR) [50]. Micelle formation and micelle size of block copolymers are studied by ^{13}C-NMR, dye solubilization method, and light scattering [51, 52]. The viscosity and rheological behavior of the copolymers are measured by viscometry [53].

Dynamic scanning calorimetry (DSC) and strain-controlled rheometry are used to characterize the phase behavior and sol–gel transition of aqueous block copolymer solutions [54]. Static (SLS) and dynamic light scattering (DLS) show aggregation number of the micelles [48]. Self-assembled copolymeric structures could be certified by cryogenic transmission electron microscopy (cryo-TEM), ^{13}C NMR, and hydrophobic dye solubilization methods [55]. The cloud point of polymer can be measured by turbidimetry [56]. Other methods such small-angle X-ray scattering (SAXS) [57, 58] and small angle neutron scattering (SANS) have been also reported to investigate the copolymer systems [59].

To find out more details about PLGA-PEG-PLGA triblock copolymers with different PEG length and their aggregation behavior at various concentrations and temperatures, different methods including tube inversion method, turbidimetry, dynamic light scattering (DLS), rheology, rheo-small angle light scattering (Rheo-

SALS) and small-angle neutron scattering (SANS) have been applied in this research.

2.11.1. Test Tube Inverting Method

Test-tube inverting method is a simple technique to determine the phase boundary between sol and gel phases. In this method, a test tube is inverted, if the solution flows, it is defined as a sol phase; if no visible flow occurs within 30 seconds the system is considered in the gel state. As flow is depending on some parameters such as temperature, amount of solution, tilting rate and the diameter of the test tube, it is necessary to fix the test parameters before measurements [34, 60].

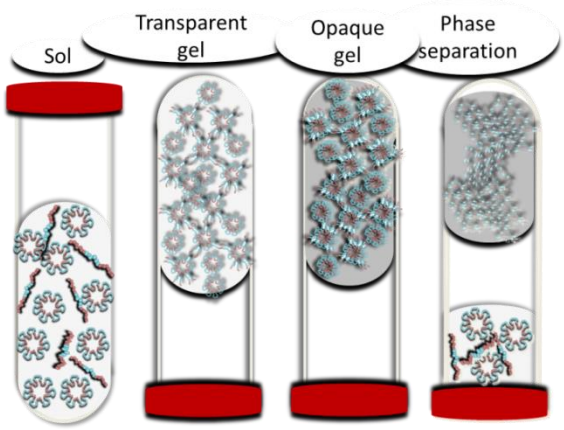

Figure 2.10 Illustration of the gel point in triblock copolymers at different temperatures.

2.11.2. Turbidimetry

Turbidity is a measure of cloudiness of a sample and indicates how much the solute hinders the passage of light. This optical technique, generally referred to as

turbidimetry, is considered as a transmission type of measurement, in which the detector is optically in line with the light source (Figure 2.11). The particles in polymer solution scatter the transmitted light away from the in-line detector, and consequently cause a loss in light intensity falling on the detector. This decrease in light intensity is measured and converted to optical density units relative to a solution without particles. The turbidity measurement gives insight into structure change of the systems on a global scale and also the thermodynamic and associative properties of polymer solutions. A steep increase in the turbidity of polymer solutions may be due to the changing of thermodynamic conditions of the system.

The scattered light of particles is measured and transformed to optical density units relevant to a solution without particles by eq. 1. Where τ is turbidity, L is the path length of the light in the cuvette; I_t and I_0 are the intensities of the transmitted and incident light respectively [56].

$$\tau = \left(\frac{-1}{L}\right) ln\left(\frac{I_t}{I_0}\right) \qquad (1)$$

The incoming light goes through the sample where the sample is placed on the surface of turbidimeter that coated with metal (mirror) (Figure 2.12). The sample without particles reflects the incoming beam from the surface of the mirror and no signal will be indicated by the optical detector (which has been placed right above the sample cell). The sample with particles scatters the incoming beam, and the signals are detected by optical detector. The incipient change in the turbidity of sample can be determined by plotting the value of turbidity versus temperature.

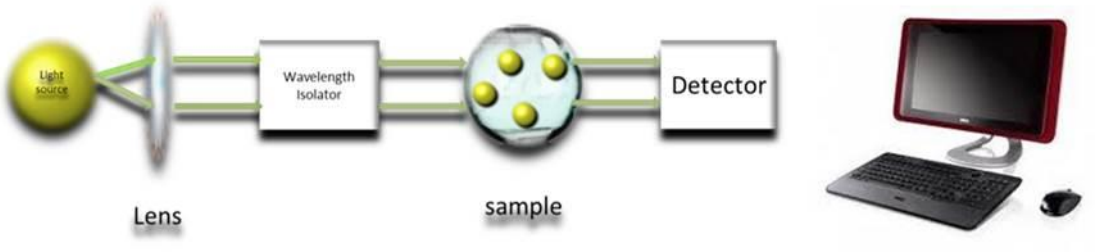

Figure 2.11 Schematic illustration of a turbidimeter.

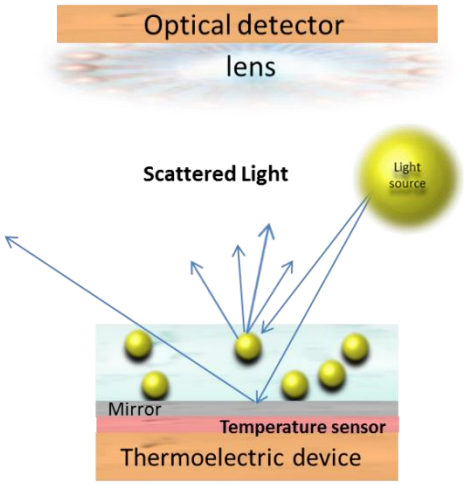

Figure 2.12 Schematic illustration of a cloud point analyzer.

2.11.3. Rheology

Rheology is described as the process of formation and breaking down of matter in response to an exerted stress. If the viscosity of a sample changes with the temperature, not with the strain rate it is known as Newtonian fluids. While for a large class of fluids, the viscosity changes with the strain rate (or relative velocity of flow) are called non-Newtonian fluids. The word rheology comes from rheo, from the

Greek word for flow, and –ology, meaning study of[61]. The rheological features of solutions are dominant properties that can be quantified to characterize its treatment, and the special rheological features of a certain solution characterized by the respond of a liquid to a forced shearing flow. The measurement of rheological features gives insight into elastic and viscous properties of the system on a macroscopic scale. Viscosity is one of the features that investigated in rheology, which the resistance of fluid to flow is determined. The Power law model of $\eta\,\dot{\gamma}^{(\alpha-1)}$ is a suitable fit equation that can describe the scaling of viscosity with shear rate where $\alpha = 1$ for a Newtonian system, $\alpha > 1$ for a shear thickening system (the viscosity increase at low shear rates) and $\alpha < 1$ for a shear thinning system (the viscosity decease at low shear rates because the associations disrupt at high shear rate). Due to the uniform shear rate, the plate and cone rheometer is suitable for studying the influence of shear rate on the rheological features of polymeric systems. The basic geometry is shown schematically (Figure 2.13). The shear rate is almost the same everywhere in the sample provided the gap angle θ_0 is small. The sample is placed between flat stationary plate and a rotating cone. Each point is determined while the cone is rotating at various shear rates. If the sample under studying has a low viscosity, high rotational accelerations are often essential to generate sufficiently large torques to be measured accurately.

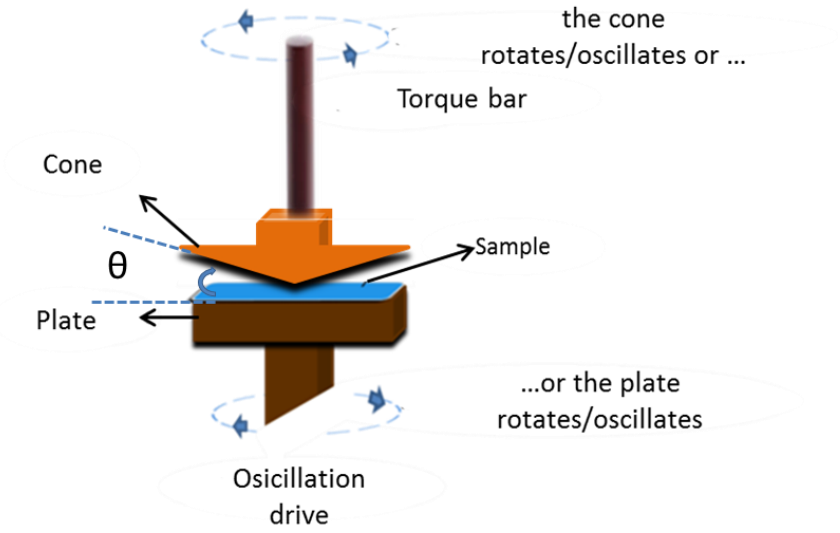

Figure 2.13 Schematic picture of the rheometer.

2.11.3.1. **Oscillatory Shear Measurements**

To understand the dynamic and structural features of the sample, oscillatory rheological measurements are applied. The viscous-like and elastic-like behavior of the sample at various temperatures can be determined by this method. The base of oscillatory rheology is to produce a sinusoidal shear deformation on the sample and measuring the response to the stress. If the sample is placed on the bottom plate (the bottom plate is stationary and the upper plate rotates by a motor) the time dependent strain is determined $\gamma\,(t)$, while the sample is imposed on the top plate, by measuring torque the time dependent stress is determined $\sigma\,(\mathrm{t})$. A single frequency is applied on different materials to measure the time dependent stress and observe different behaviors Stress is proportional to the strain deformation for an ideal elastic material $(\delta = 0)$, whereas in an ideal viscous material stress is

proportional to the rate of strain ($\delta = \pi/2$). In the case of viscoelastic materials, which simultaneously show liquid-like and solid-like characteristics, both in-phase and out-of-phase response contributions are observed. In fact, the total stress response shows a phase shift δ with respect to the applied strain deformation that lies between solids and liquids, $0 < \delta < \pi/2$. The stress and strain waveforms are displayed in Figure 2.14.

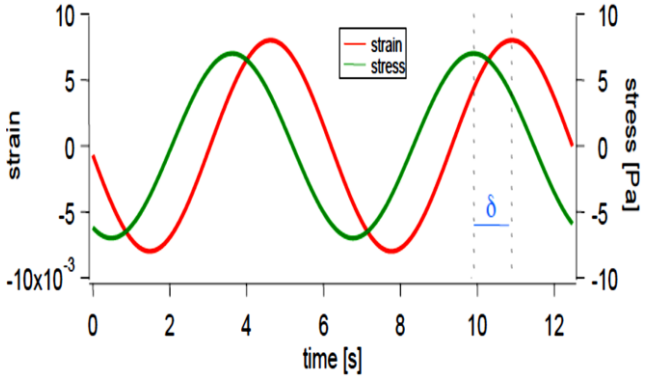

Figure 2.14 Illustration of oscillating strain and stress respond.

The viscoelastic behavior of the system at ω is characterized by the storage modulus, $G'(\omega)$, and the loss modulus, $G''(\omega)$, which respectively characterize the solid-like and fluid-like contributions to the measured stress response. The stress and strain can be written as:

$$\gamma = \gamma_0 \, sin(\omega t) \tag{2}$$

$$\sigma = \sigma_0 \;\; sin(\omega t + \delta) = \; \sigma_0 \, cos(\delta) \, sin(\omega t) + \sigma_0 \;\; sin(\delta) cos(\omega t) \tag{3}$$

Where γ_0 and σ_0 are the maximum amplitudes for the strain and stress, ω is the frequency in radians per second ($\omega = 2\pi\nu$), and t is time.

The stress may be written as:

$$\sigma = \gamma_0 \left[G'(\omega)\, sin(\omega t) + G''(\omega) cos(\omega t)\right] \quad (4)$$

Where $G'(\omega)$ is the storage modulus and $G''(\omega)$ is the loss modulus. The ratio of G'' to G' gives a measure of relaxation and is called the loss tangent:

$$tan\delta = \frac{G''}{G'} = tan(n\pi/2) \quad (5)$$

δ is the phase difference in radiation between the peak value of the stress, and the peak value of the strain, which is constant with time at any given frequency[62].

2.11.3.2. **Determination of the Gel Point**

Gel point can be specified by oscillatory shear measurements. Corresponding to the model of Chambon and Winter, the gel point is determined based on frequency-independent value of tan δ versus time (for chemical gels) or temperature (thermoreversible gels). In this regard, the following power-law of G' and G'' is valid:

$$G'(\omega) \sim G''(\omega) \sim \omega^n \quad (6)$$

Where n $(0 < n < 1)$ is the relaxation exponent.

The gel point is defined where tan δ is plotted versus the gel forming parameters (e.g. time or temperature) at different frequencies and the point that tan δ is independent of frequency is measured. By plotting G' and G'' versus frequencies at different temperatures, the gel point can be determined where G' and G'' versus ω have the same slopes. Gel point can be also determined by plotting the “apparent” viscoelastic exponents n' and n'' ($G' \sim \omega^{n'}$, $G'' \sim \omega^{n''}$) obtained from the frequency dependence

of G′ and G″ at different stages during gelation process and observing a crossover where $n' = n'' = n$ [61].

2.11.3.3. Gel Strength Parameter

To characterize gel stiffness at the gel point, the gel strength parameter (S) is defined; which depends on cross-linking density and molecular chain flexibility. The value of n and S for an incipient gel can be determined from power law modeling of the frequency of the absolute value of the complex viscosity [63].

$$G' = \frac{G''}{tan\delta} = S\omega^n \Gamma(1-n)cos\delta \ (2) \qquad (7)$$

Where $\Gamma(1-n)$ is the Legendre gamma function.

2.11.3.1.1. Theoretical Models for the Interpretation of n

To predict the relaxation exponent, some theories have been developed. The growing clusters, which appear as the connectivity increases near the gelation threshold, may be defined as the fractal geometry on the length scales between the monomer size and the correlation length of connectivity.

The structure of the incipient gel can be explained by a fractal dimension, d_f,

$$R_g \ d_f \sim M \qquad (8)$$

Where R_g is the radius of gyration and M is the mass of a molecular cluster. A dynamical scaling analysis of flexible fractals in the Rouse limit (no hydrodynamic interaction), taking into account the effect of screening of excluded-volume and

hydrodynamic interactions but ignoring entanglement effect, yield a monodisperse solution of polymers of fractal dimension d_f with a viscoelastic exponent of,

$$n = \frac{d_f}{(d_f + 2)} \tag{9}$$

If the range that the fractal dimension is $1 \leq d_f \leq 3$, the calculated relaxation exponent from eq. 9 is restricted to $1/3 \leq d_f \leq 3/5$. If the effects of polydisperse clusters near the gel point are considered, the relationship for non-entangled system would be:

$$n = \frac{d_f(r-1)}{(d_f + 2)} \tag{10}$$

Where r is the scaling exponent for the cluster-size near gel point: $r = 1 + d/d_f$where d $(d = 3)$ is the space dimension. Values of n in the total range $0 < n < 1$ have been reported in many of oscillatory shear studies on incipient gels of different temperaments. The model of Muthukumar describes with increasing the excluded volume effect, the strand length between cross-linking points of incipient gel networks increases. If the excluded volume interaction is fully screened, the relaxation exponent for a polydisperse system can be expressed as:

$$n = \frac{d\left(d + 2 - 2d_f\right)}{2\left(d + 2 - d_f\right)} \tag{11}$$

$$1 \leq d_f \leq 3;\ 0 \leq n \leq 1$$

$$d_f = 2.5 \Rightarrow n = 0;\ d_f = 1.25 \Rightarrow n = 1$$

In the case of unscreened excluded volume interactions:

$$n = \frac{d}{(d_f + 2)} \tag{12}$$

n varies from 1 to 0.6 as d_f varies from 1 to 3. Incipient gel networks with high values of n have low fractal dimensions and are considered as “open” networks, while networks with low values of n have higher fractal dimension and called “tight” networks (Figure 2.15). The figure below shows tight and open structures [64].

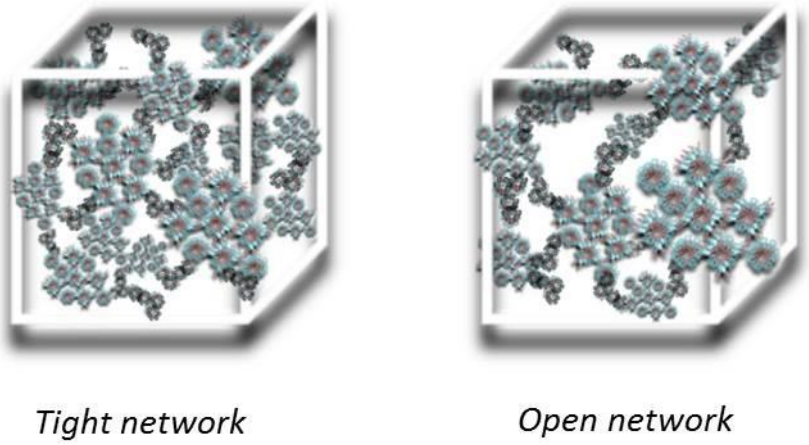

Figure 2.15 An illustration of a tight and an open network.

2.11.4. Rheo-Small Angle Light Scattering (rheo-SALS)

Rheo-small angle light scattering is one of the most extensively applied techniques for studying structural features simultaneously with the rheological behavior. This technique provides information about structural changes of complexes on a global dimensional scale $(0.0005 \leq q\ (\text{Å}^{-1}) \leq 0.005)$ under the influence of shear flow. An incoming initial laser beam, which induces the angular distribution of the scattered light, is analyzed according to its angle and intensity. Structural information can be

obtained from the scattered light distribution with some assumptions. Fluctuations in the anisotropy of the polarizabillity and fluctuations in the polarizabillity are dependent on the orientation and the concentration between ingredients of a multiphase system. To make polarized and depolarized experiments possible, a polarizer is placed above the sample and an analyzer is placed below the sample. The sample is located between transparent plates and the beam is deflected by prism and passed through the sample. The effect of multiple scattering is low when the sample becomes turbid due to the small distance between the plates. A CCD camera with a Pentax lens was employed and stored the scattered pictures and SALS software program applied to analyze the images. The refractive index was measured at different temperatures with an automatic refractometer (Model PTR 46). Temperature control was performed by a liquid thermobath. The absolute value of the scattering vector is defined by the following equation:

$$q = \frac{4\pi}{\lambda}.sin\left(\frac{\theta}{2}\right) \qquad (13)$$

Where λ is the wavelength of the incoming radiation; θ is the scattering angle, n is the refractive index of the medium [65].

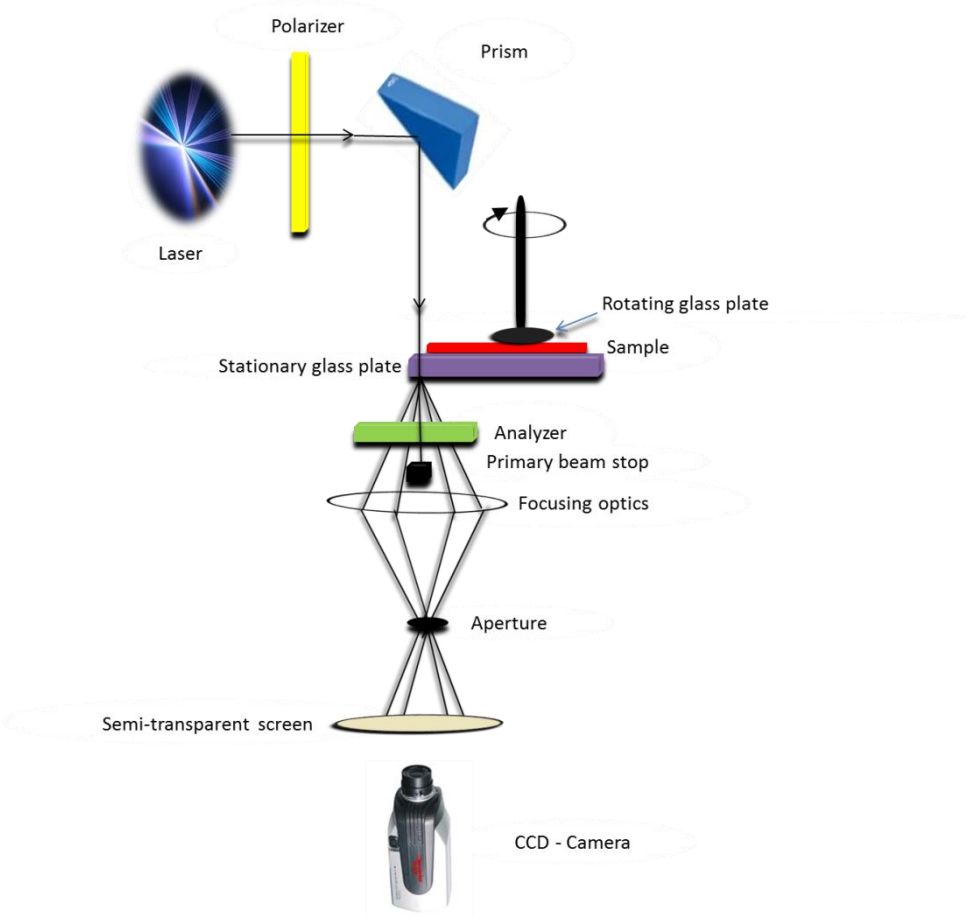

Figure 2.16 Schematic picture of rheo-SALS.

2.11.5. Small Angle Neutron Scattering

In small angle neutron scattering (SANS), neutron beam is scattered by the sample and analyzed to provide information about the size, shape and orientation of some component of the sample. This powerful technique allows to examine large-scale heterogeneous structures between 1 and $100\ nm$. In light scattering measurements we investigate on a wave vector (q) range of approximately $0.0005 \leq q\ (\text{Å}^{-1}) \leq 0.005$, whereas with SANS structural changes are studied on $0.005 \leq q\ (\text{Å}^{-1}) \leq 0.8$ range. According to wave vector range, more information on global dimensions

can be found from light scattering measurements, while the structure on local scales are obtained from SANS. Perhaps the most important fact is with minor adjustments to account for the different types of radiation, the same basic equations and laws (for example, Guinier, Zimm, Kratky and Porod) can be used to determine data from any of scattering techniques. SANS probes a sample on the length scale $2\pi/q$ which is a central quantity in the scattering experiments and the wave vector q is defined according to eq 13. The length scale (local or global scale) is determined by the value of the inverse of the wave vector $2\pi/q$.

Due to sensitivity to both the local and global scales, from micron to nanoscale can be covered. A dimensionless quantity qL is defined in the scattering measurements, where L is a characteristic length $(R_g \; or \; R_h)$ in the dilute regime, and $(\xi_S \; or \; \xi_D)$ in the semidilute region. The low value of wave vector (q), when $qL < 1$ (Guinier region) the scattered intensity is considered on a global dimension, while in the regime $qL >> 1$ (the fractal region), inner structure of the polymer is observed from the length scale q^{-1}. Some associating systems show a large increasing in the scattered intensity at low q values due to the large aggregation. This upturn is usually described by power law with an exponent in the range of 2-4 (an exponent of 4 is characterristic of Porod scattering). In the fractal region$qL >> 1$, the q dependency of the scattered intensity can also be described by a power law

$$I(q) \sim q^{-d_f} \qquad (14)$$

Where the fractal dimension d_f is the slope of the structure factor in the power law. The value of d_f represents the local conformation of the polymer chains. A value of

$d_f = 3$ shows a spherical or compact structure of the chains. For random coil in good and θ condition the fractal dimension is equal to 1.7 and 2 respectively. A value of $d_f = 1$ is an indication of a rod-like conformation.

Guinier approximation:

$$I(q) \propto exp\frac{-q^2 R_g^2}{3} \qquad (15)$$

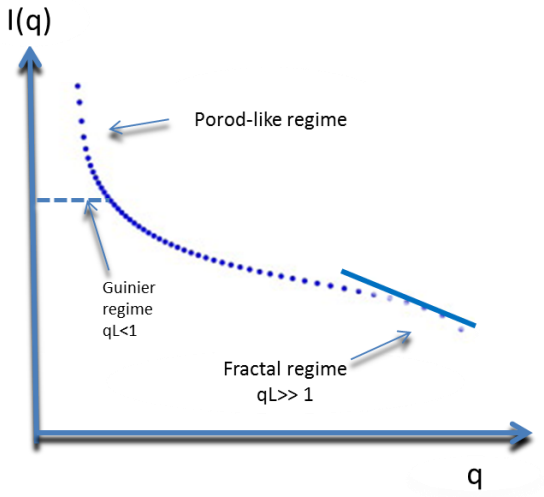

Figure 2.17 Illustration of the SANS scattering intensity over an extended q range.

2.11.5.1. **Core – Shell Micelles**

For a more detailed analysis of scattering results, we need to postulate a structure for the aggregates. The structure of the micelles is expected to be like Figure 2.18, where the insoluble PLGA blocks cluster together and are surrounded by a shell of the soluble PEG chains, much like a polymer brush. From a distance, the aggregate is simply a sphere. Closer up, it is a spherical core, with a shell on the surface. We will consider our solution to contain some concentration of these micellar structures,

with a “dry” core that contains only polymer, and a shell that contains extended chains and some quantity of solvent. The scattered intensity from a collection of monodisperse particles can be written as:

$$I\,(q) = n_p P(q) S(q) \qquad (16)$$

Where n_p is the number density of particles, P (q) is the form factor, and S (q) is the structure factor. The scattering amplitude is defined as a Fourier integral of the scattering length density difference between any point in the particle and the solvent:

$$f_{k(q^{\rightarrow})} = \int [\rho_k(\vec{r}) - \rho_{solv}]\; e^{\overrightarrow{iq.r}} \overrightarrow{dr} \qquad (17)$$

For the case of a core-shell sphere:

$$P(q) = \frac{scale}{V_s}\left[\frac{3V_c(\rho_c - \rho_s) j_1(qr_c)}{qR_c} + \frac{3V_s(\rho_s - \rho_{solv}) j_1(qr_s)}{qR_s}\right]^2 + bkg \qquad (18)$$

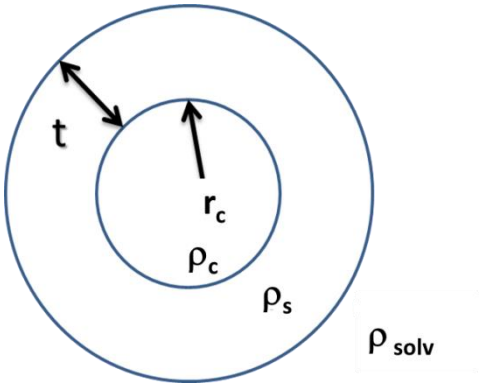

Figure 2.18 Schematic illustration of core-shell structure, where r_c and t are the radius of the core and thickness of the shell. The parameters ρ_C, ρ_s and ρ_{solv} are just the scattering length density (SLD) of the core, shell and solvent (D2O), respectively.

Where $j_1(x) = (\sin x - x \cos x) / x_2$, $r_s = r_c + t$ and $V_i = (4\pi / 3) R_i^3$ .The parameters r_c and t are the radius of the core and thickness of the shell, respectively. V_s and V_c are the volumes of the shell and the core, and bkg is just the background.

The values ρ_C, ρ_s and ρ_{solv} are just the scattering length density (SLD) of the core, shell and solvent (D_2O). j_1 is a standard mathematical function (Bessel function), and scale is directly related to the concentration. $P\,(q)$ is the form factor for these particles, which contains all of the information about the shape and scattering contrast of the particle. The structure factor, $S\,(q)$, describes the relative positions of the micelles in solution. If the solution is dilute, the micelles do not interact with each other (think of an ideal gas of micelles), then the structure factor, $S\,(q) = 1$ for all q-values. As the solution becomes more concentrated, the micelles "feel" the presence of each other, excluding the volume of solution that other micelles can occupy. This is reflected in the relative positions of the micelles in the solution. This is the model that was fitted to the SANS data, giving the core radius and shell thickness of the particles. However, the core size is the most accurate, because the shell will often be very open (diluted), thus producing much less contrast than the core [66].

3. Experimental Section

In this study, PLGA-PEG-PLGA triblock copolymer aqueous solutions with different PEG length have been characterized by means of a wide range of techniques ranging from a simple "test tube inverting method" for the gel point, Turbidimetry, Rheology, Rheo-small Angle Light Scattering (rheo-SALS), Dynamic Light Scattering (DLS) and Small-Angle Neutron Scattering (SANS).

3.1. Materials

D, L-Lactic acid (LA) and glycolic acid (GA) from Sigma-Aldrich were recrystallized from ethyl acetate, dried under vacuum and stored at -18°C before using. Poly (ethylene glycol), with PEG length 1000, PEG length 1500, and tin (stanneous) 2-ethylhexanoate [$CH_3 (CH_2)_3 CH (C_2H_5) CO_2]_2 Sn$ were purchased from Sigma-Aldrich and used without further purification. All other chemicals were reagent-grade and used as purchased.

3.2. Synthesis

The ABA-type triblock copolymers, poly[(D,L-Lactic acid-co-glycolic acid)-*b*-poly(ethylene glycol)-*b*-poly(D,L-lactic acid-co-glycolic acid)], abbreviated as PLGA-PEG-PLGA were prepared by ring-opening polymerization (ROP) of D,L-lactic acid and glycoli acid with PEG as the initiator and stannous octoate ($Sn(Oct)_2$) as the catalyst [5]. Figure 3.1 shows feed ratios of the PEG/GA and LA/GA were used to adjust the composition and molecular weight.

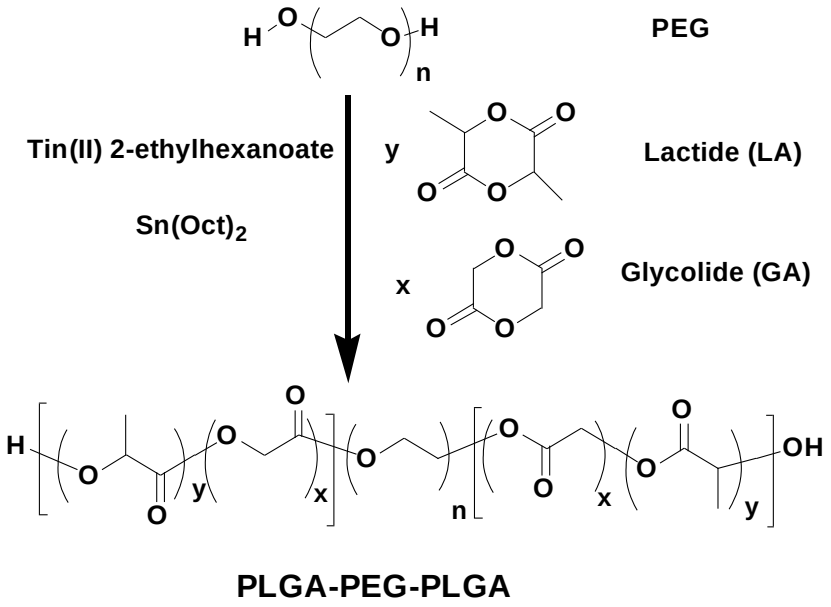

Figure 3.1 Synthetic scheme of PLGA-PEG-PLGA triblock copolymers.

The detailed synthesis process of copolymer $PLGA_{1170}$-PEG_{1000} -$PLGA_{1170}$ can be described as follow: 15 mmol of the polyethylene glycol with M_n=1000 g/mol was dried under dry argon atmosphere in a three-necked flask (5 mm Hg) and stirred at 120°C for 2 hours. Then the temperature of the flask was decreased to 80°C and kept under argon. DL-Lactic (28.4 g, 0.197mol) and glycolic (7.6 g, 66 mmol) were added in the mole ratio of 3:1, respectively, and the reaction mixture was heated under vacuum for another 30 min. After complete melting of the DL-lactic and glycolic, 0.02 g of $Sn(Oct)_2$ were added and the reaction mixture was further heated at 150°C for 12 hours. The unreacted monomers were removed under vacuum. The flask was then cooled down to room temperature, and the residue was dissolved into ice-cold water in the range of 4-8°C. After complete dissolution, the polymer solution was

heated to 70 – 80°C to effect precipitation of the polymer and to remove water-soluble low-molecular weight polymer and unreacted monomer. Precipitated polymer was isolated by removing the supernatant and re-dissolving in ice-cold water and heated to induce precipitation. The precipitation process was repeated three times. Finally, the polymer was dissolved in a minimum amount of water and lyophilized. The resulting PLGA-PEG-PLGA copolymer was collected and kept at -18°C.

Figure 3.2 presents the chemical structure and composition of the ABA triblock copolymers. The compositions were determined by their ^{1}H NMR spectra in $CDCl_3$ solutions containing Tetra Methyl Silane (TMS) as reference at 25°C (Bruker AVANCE DPX 300 MHz spectrometer).

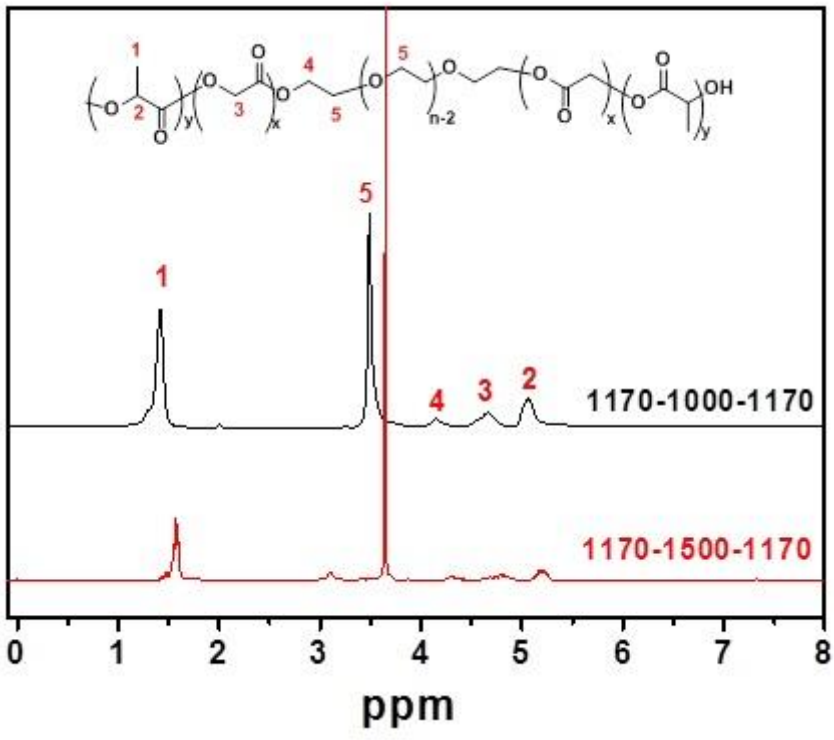

Figure 3.2 ^{1}H NMR spectra of PLGA-b-PEG-b-PLGA triblock copolymers ($CDCl_3$-d as solvent, 300 MHz).

The molar composition of each sample was calculated by comparing the integral area of the PEG methylene peak (**5**) (δ = 3.65 ppm), the LA single proton (**2**) (δ = 5.15 ppm) and the GA methylene group (**3**) (δ = 4.8 ppm). The entire repeating units of LA/GA(EG (2x/2y/n) were estimated to be 25/9.46/22 and 24.8/9.54/34 for PLGA-PEG_{1000}-PLGA and PLGA-PEG_{1500}-PLGA derivative polymers, based on the calculations, the numbers of repeating units of the ethylene glycol of PLGA-PEG_{1000}-PLGA and PLGA-PEG_{1500}-PLGA are 22 and 34 respectively, as shown in table 3.1.

Table 3.1 Physical parameters of synthesized PLGA-PEG-PLGA triblock copolymers.

Polymers	PEG (M_n, g/mol)	LA/GA (Feed)	LA/GA/EG/GA/LA (y/x/n/x/y)	M_n (NMR)
PLGA-PEG-PLGA	1000	2.65 (3)	12.5/4.73/22/ 4.73/12.5	3348 (1174-1000-1174)
PLGA-PEG-PLGA	1500	2.77(3)	12.4/4.77/34/ 4.77/12.4	3840 (1170-1500-1170)

3.3. Sample Preparation

All solutions were prepared by weighing the amount of polymer, based on the desired concentration, and dissolved in phosphate buffer with pH= 7.4.

Solutions for DLS measurements were filtered in an atmosphere of filtered air through a 0.8 μm filter (Gelman Sciences) directly into pre-cleaned 10-mm NMR

tubes (Wilmad Glass Co.) of the highest quality. For the neutron-scattering measurements, solutions were prepared in heavy water (D_2O) as a solvent instead of H_2O primarily in order to increase the scattering contrast between the solvent and copolymer and, secondly, to reduce incoherent scattering which adds to the background [67]. The experiments were carried out in two different polymer concentrations corresponding to 1 wt% (dilute regime) and 20 wt% (semidilute regime). The solutions were allowed to stand in an incubator and homogenized by slow stirring, at low temperature (10°C) to avoid phase separation, for 24 hours.

3.4. Test Tube Inverting Method

Aqueous solutions of the copolymers were prepared in phosphate buffer with PH=7.4 in various concentrations. 2 ml of each solution was transferred to glass tubes. The tubes were kept in the water bath and heated up from 4°C to 60°C. The sol-gel transition temperature was determined by flow or no-flow criterion over 30 s. The temperature was controlled at the heating rate of 0.2°C/min, and the transition temperature was monitored at an accuracy of $\pm$1°C [68].

3.5. Turbidimetry

The turbidity of dilute and semidilute PLGA-PEG_{1000}-PLGA, PLGA-PEG_{1500}-PLGA and the mixing of the two copolymers solutions were monitored with the aid of an NK60-CPA cloud point analyzer from Phase technology, Richmond, BC, Canada.

The light beam from an AIGaAS light source (654 nm) was passed through 0.15 mL of the sample, which was placed by a micropipette onto a special glass plate that was covered with a slim metallic layer of very high reflectivity (a mirror). The apparatus is equipped with a temperature unit (Peltier plate) that has responsibility to adjust the temperature of the sample. Evaporation might occur during the temperature scanning measurement; consequently a thin layer of silicon oil was applied in order to minimize evaporation.

The relation between the signal (s) and turbidity (τ) of the samples was calculated according to equation 19 [56],

$$\tau = 9.0.10^{-9} S^{3.751} \qquad (19)$$

The heating rate in each measurement is 0.2°C /min.

3.6. Small Angle Neutron Scattering

The small angle neutron scattering measurements were carried out at the SANS installation at the IFE reactor at Kjeller, Norway. The instrument is equipped with a liquid hydrogen moderated thermal neutron spectrum toward longer wavelengths. In this measurement, fast neutrons (cutoff at a wavelength of $\lambda = 4\,\text{Å}$) and the γ radiation have to remove, so liquid- nitrogen- cooled 15 cm long Be- and Bi- filter is fixed in the light path. Wavelength λ was set by means of a velocity selector, using a high FWHM for the transmitted beam ($\Delta\lambda/\lambda = 20\,\%$), and maximized flux on the sample. He-filled RISØ- type detector with 58 cm diameter is mounted in 3.5 m long shielded tank.

The solutions were filled in 2 mm Hellma quartz cuvettes, which were equipped with stoppers. The measurements were carried out at different temperatures. A good control of temperature is submitting with a rotatable 7-position located inner a steel chamber. For air sensitive samples the camber can be depleted to decrease air scattering.

Standard reductions of the scattering data, including transmission corrections, were conducted by incorporating data collected from empty cuvette, beam without cuvette, and blocked-beam background. When relevant, the data were transformed to an absolute scale (coherent differential cross section ($d\Sigma/d\Omega$)) by calculating the normalized scattered intensity from direct beam measurements [69].

3.7. Rheometer

The oscillatory shear measurements were applied in a Paar-Physica MCR 301 rheometer using a cone-and-plate geometry, with a cone angle of 1° and a diameter of 75 mm. The instrument is equipped with a temperature unit (Peltier plate) to give the temperature control within (± 0.05°C). All rheological data were investigated as a function of strain amplitude to ensure that the measurements were conducted in the linear viscoelastic region. The solutions were placed on the plate and an oil with a low viscosity has been applied to avoid the evaporation of the solvent (this layer of oil does not affect the viscoelastic respond of the sample).

3.8. Rheo-SALS

Combined rheological and small angle light scattering experiments during shear flow were performed using the Paar-Physica MCR 300 rheometer, equipped with a specially designed parallel plate-plate configuration (the diameter of the plate is 43 mm) in glass. The instrumentation for the rheo-SALS experiments was purchased from Physica-Anton Paar. In all measurements a 10 mW diode laser operating at a wavelength of 658 nm was used as the light source.

4. Results and Discussion

4.1. Dilute Solutions

4.1.1. Turbidimetry

At low temperature, a unimer-micelle transition occurs and with rising temperature intermicellization takes place with the evaluation of loose micellar clusters [70]. On the other hand, the hydrophobicity of copolymers increases and they become more sticky above their cloud point (CP). CP is defined as the temperature at which the turbidity increases drastically and macroscopic phase separation occurs in the solution [71]. Therefore, the micelles aggregate because of attractive interactions and form the large aggregations, which are responsible for enhancement in turbidity.

In Figure 4.1, the temperature evolution of the turbidity for dilute PLGA-PEG-PLGA solutions with different PEG length is displayed. The incipient rise of the

turbidity with increasing temperature takes place at higher temperatures when the hydrophilic chains become longer due to a higher temperature needed to obtain the required stickiness for aggregation of the species. The Figure presents the turbidity transition of the PLGA-PEG_{1000}-PLGA solution is located at lower temperature (27°C), while in the case of copolymers with longer PEG length it is located at higher temperature (37°C). At a given concentration, the strong upturn of the turbidity at high temperatures indicates that unimers form micelles and intermicellar structures are formed as the temperature rises. This is more dominant for the copolymer with shorter PEG length. This is due to the formation of unstable micelles and intermicellar structures at relatively lower temperatures in comparison with the copolymer with longer PEG length. On the other hand, the effect of enhanced hydrophobicity at higher temperatures is more pronounced for copolymer solutions with shorter length of hydrophilic block. After the turbidity passes through a maximum, it decreases again.

According to the SANS results mentioned part 2.1.1, the aggregates are more easily formed for copolymer with shorter PEG length due to the more hydrophobic character of copolymers which leads to more unstable micelles (ellipsoids) at lower temperatures. The copolymer with shorter PEG length is formed an extended oblate shape of micelle at temperature 30°C, which will easily aggregate. While the copolymer which leads to with PLGA-PEG_{1500}-PLGA solution form the stable micelle below 40°C. It is evident that shorter PEG length results in a turbid solution at lower temperatures.

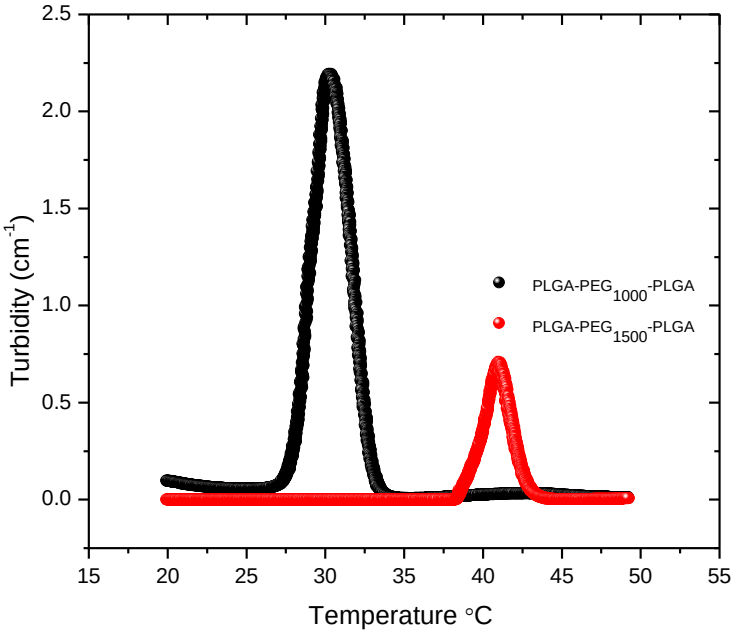

Figure 4.1 Turbidity versus temperature for 1 wt% PLGA-PEG1000-PLGA and PLGA-PEG1500-PLGA solutions from 20 °C to 50°C.

4.1.2. Small Angle Neutron Scattering

The q dependencies of the scattering intensity for 1.0 wt% PLGA-PEG_{1000}-PLGA and PLGA-PEG_{1500}-PLGA solutions at different temperatures are displayed in Figure 4.2 in a double logarithmic scale. The intention of this study was to probe possible changes of the copolymer's structures with different PEG lengths at various temperatures in aqueous solutions. The SANS spectra for these two systems exhibit quite different profiles, which indicate that the PEG length have affect the structures.

No visible change of the intensity can be observed over the whole range from 10°C to 35°C for the copolymer with longest PEG (Figure 4.2 a). The results show

the shape of micelles is spherical (apart form a possible slight distortion at 30-35°C) and the core size of micelles is reduced by increasing the temperature.

Different behavior is observed for the copolymer with shorter PEG length (Figure 4.2 b). The slope of the plot at low q values shows that micelles are not spherical, but they are ellipsoids at 20°C. The PLGA-PEG_{1000}-PLGA system has a non-spherical, most likely prolate, equilibrium shape at 10°C, which shifts into an extended oblate shape at 20°C. This might explain the reason of significant signal dropping at temperature 30°C and the intensity has basically been disappeared at 35°C. Very large extended (ellipsoids) have been created upon increasing temperature in the solution, which will easily aggregate and sediment out of the scattering volume. For PLGA-PEG_{1500}-PLGA, a good fit with core-shell model was observed at all measured temperatures. This behavior is very different from the PLGA-PEG_{1500}-PLGA sample, which creates spherical micelles that are stable in this temperature range. This phenomenon suggests that PEG length affects the local structure of the copolymer solutions.

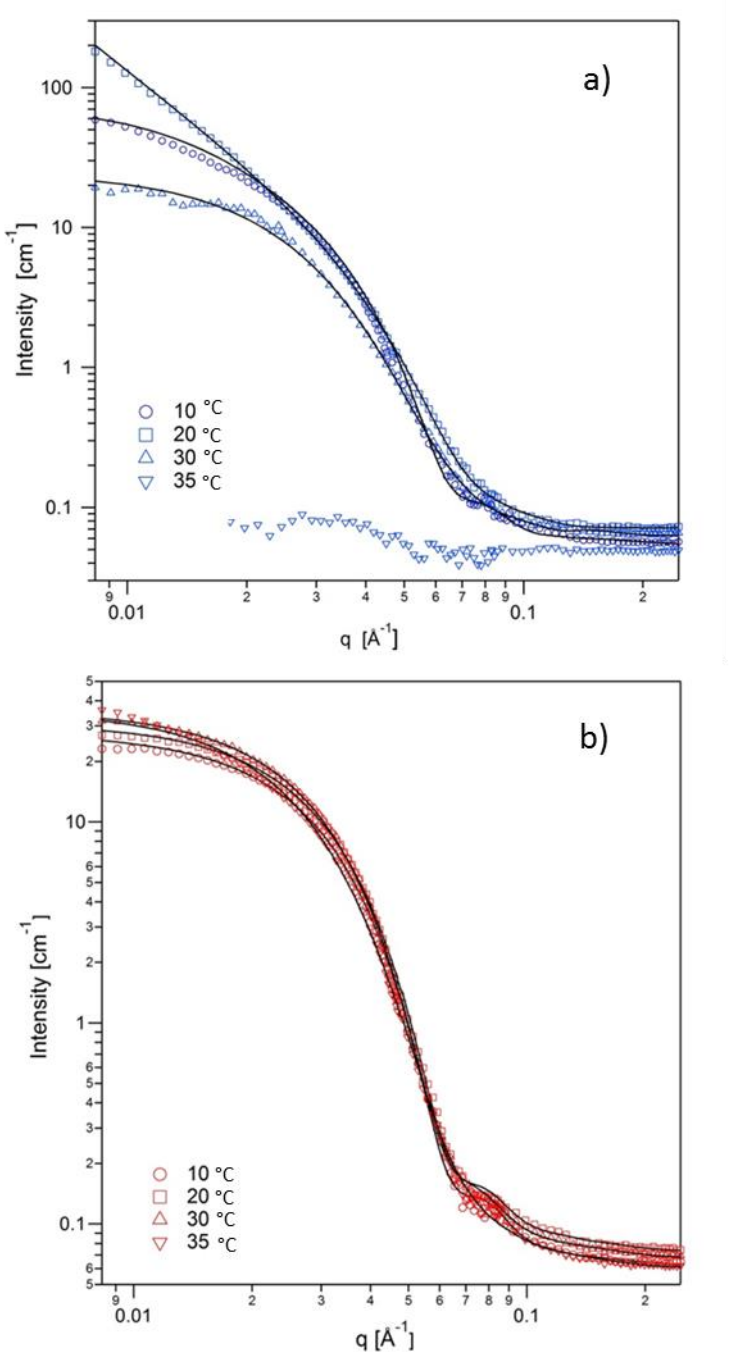

Figure 4.2 SANS scattered intensity plotted versus the scattering vector q for 1 wt% a) PLGA-PEG1000-PLGA and b) PLGA-PEG1500-PLGA samples at different temperatures in dilute region.

4.2. Semidilute Solutions

4.2.1. Test Tube Inverting Method

PLGA-PEG_{1000}-PLGA triblock copolymer in phosphate buffer (PH = 7.4) exhibits three physical states depending on the concentration: free micelles in solution, hydrogels (transparent and opaque gel), and precipitates from below 12°C to higher 34°C.

The temperature–concentration phase diagram (Figure 4.3.) of the solution shows that the sol–gel transition temperature decreased by increasing concentration of the triblock copolymer. PLGA-PEG_{1000}-PLGA with different concentration (10, 15, 20, 30 wt%) has been considered. By increasing the copolymer concentration from 10 wt% to 30 wt%, transition temperature of the sol to transparent gel was decreased and transparent gel to sol was increased.

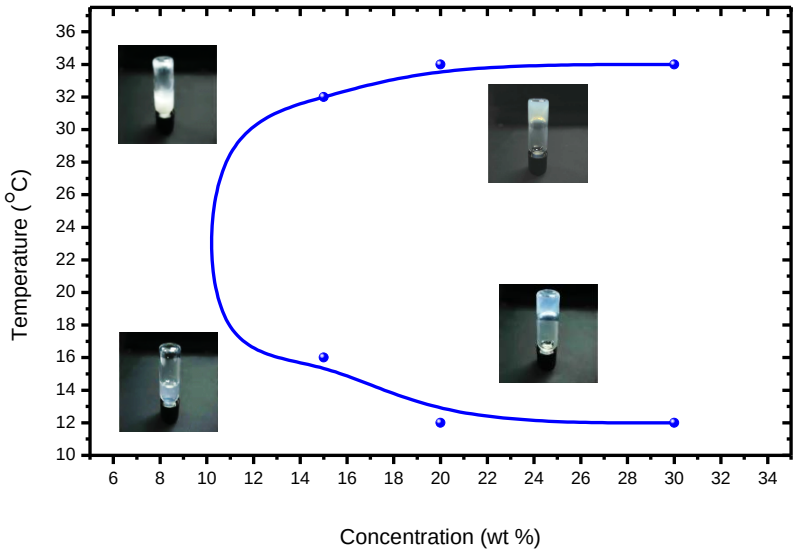

Figure 4.3 Illustration of a temperature–concentration phase diagram of the solution PLGA-PEG1000-PLGA.

The formed micelles have hydrophobic core (PLGA) and hydrophilic shell (PEG) in aqueous solutions. Increasing the concentration and raising temperature above LCST for PLGA, these micelles might also aggregate and form bridged micelles. So a gel-like network is observed [72, 73]. The sol to gel transition occurs when the hydrophobic interaction is strong enough to introduce a net inter-micellar attraction. It leads to aggregation of the micelles, possibly mediated by triblock chains spanning more than two micelles.

At higher temperatures the micelles are likely to grow leading to a precipitation that depends on concentrations may appear like an opaque gel. This behavior was proved by rheometer and SANS. The PEG length effect is especially important when an amphiphilic block copolymer has a subtle balance between hydrophilicity and

hydrophobicity. In the end, the gel network disrupts and solution disassociate into an aqueous phase and smaller precipitated micelles.

4.2.2. Turbidimetry

As the temperature increases, the hydrogen bond becomes weaker, while hydrophobic forces among the hydrophobic PLGA segments strengthen, leading to a sol–gel transition. With increasing temperature the hydrophobicity of the polymer PLGA-PEG-PLGA increases and intermolecular interactions occur [74] and the larger aggregates form and an incipient increase in the turbidity values (CP) at a certain temperature are observed [75].

Figure 4.4 presents turbidity τ of the $PLGA_{1170}$-PEG_{1000}-$PLGA_{1170}$, $PLGA_{1170}$-PEG_{1500}-$PLGA_{1170}$ and mixtures of these copolymer solutions versus temperature at a total polymer concentration of 20 wt%. For all solutions, the turbidity passes through a maximum as the temperature rises. As concentration of the PLGA-PEG_{1000}-PLGA solution decreases in solution mixtures, the incipient increase in the turbidity is observed at higher temperature. The effect of higher hydrophobicity at high temperatures is more pronounced as the solution contains pure PLGA-PEG_{1000}-PLGA. This leads to the formation of aggregates at a lower temperature and a lowering of the cloud point. This effect for PLGA-PEG_{1500}-PLGA is less pronounced, because the number of hydrophobic segments plays a less dominant role for polymer with longer PEG length.

It is likely that at higher concentrations PLGA-PEG_{1000}-PLGA solution consists of micelles where only one of the two PLGA blocks of a chain is situated into the core, and the other is extended into the solution. However, for the, PLGA-PEG_{1500}-PLGA solutions, the PEG length is long enough that the chain finds tendency to turn back on itself; therfore both PLGA blocks can enter into the same core creating more stable micellar structures (flower-like micelles)[72]. Thus a higher temperature is required to provide with sufficient interactions between micelles in order to form the large aggregations.

We notice from the inset in Figure 4.4 that the value of the cloud point is lowest as the solution consists of pure PLGA-PEG_{1000}-PLGA with the concentration of 20 wt%. The measured cloud point of different solutions shows that the polymers with the shorter PEG length have lower value of CP; i.e, the value of the cloud point is strongly affected by the PEG length.

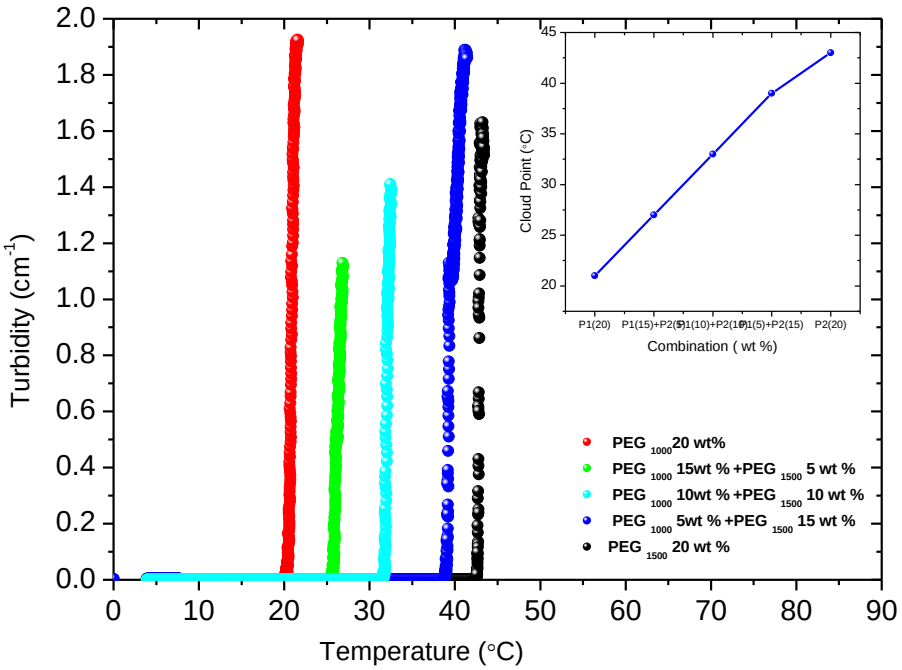

Figure 4.4 The turbidity of the PLGA-PEG1000-PLGA and PLGA-PEG1500-PLGA solutions with different PEG length and the mixtures of the two copolymers versus temperature. The inset shows effects of the PEG length on the cloud point for solutions. (P1 = PLGA-PEG1000-PLGA, P2= PLGA-PEG1500-PLGA)

Figurer 4.5 shows the turbidity versus temperature for PLGA-PEG$_{1000}$-PLGA from 4°C to 50°C in constant concentration of 20 wt%. By increasing the temperature the individual micelles below LCST (4-12°C) form the bridged micelles above LCST and the large aggregations are observed [2]. Considering the test tube inverted results, transition temperature of the transparent gel-opaque gel is 20°C. From SANS result that coming in part 3.2.5 we can see the first turbidity peak is appeared at 20°C, where we also observe a modification in the SANS pattern with disappearance of the correlation peak. At 30°C the turbidity has dropped back to a lower value, where the SANS results show transition to new structures (thin cylinders). The thin cylinders will

not produce scattering in the visible range, because the thickness is being much smaller than the wavelength. A new turbidity peak appears above 30°C, and again the SANS results show that significant change have taken place with thick cylinders that will also scatter in the visible range. Finally, between 40°C and 50°C there are only minor changes in the turbidity, similar to the SANS pattern, where the curve shape is generally the same; only a loss in overall intensity due to precipitation is observed.

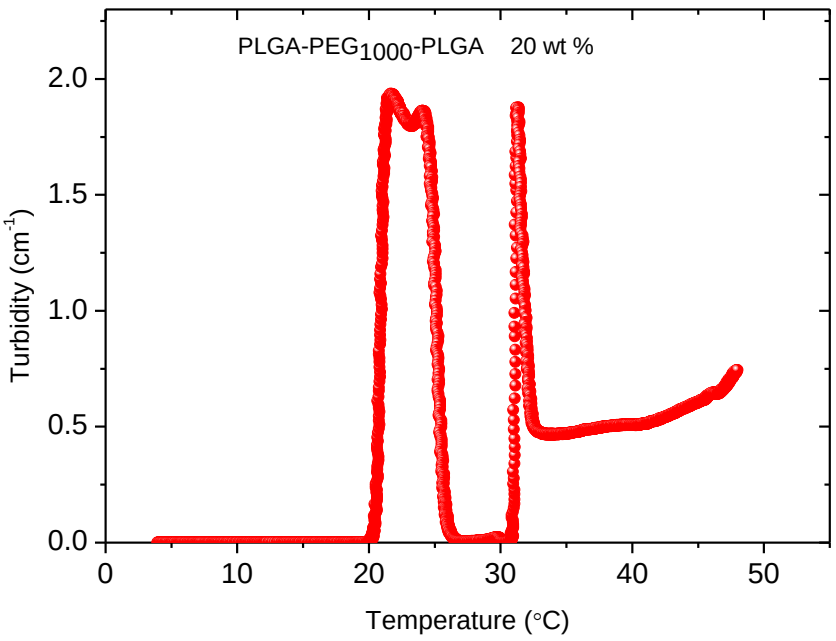

Figure 4.5 The turbidity versus temperature for 20 wt% PLGA-PEG1000-PLGA solutions from 4 to 50°C.

4.2.3. Rheology

4.2.3.1. Determination of Gel Point

The rheological properties of the copolymer PLGA-PEG_{1000}-PLGA and PLGA-PEG_{1500}- PLGA and the mixture of the copolymers at a total polymer concentration 20 wt% were scrutinized as a function of temperature by oscillatory shear measurements. By using the theory of Winter and Chambon the gel points (GP) of the samples can be determined (Figure 4.6). An alternative method to determine the gel point is to plot the "apparent" viscoelastic exponents n' and n'' versus temperature [76] (inset of Figure 4.6b) explained briefly in experimental technique (Determination of the Gel Point). These two methods yield the same gel points for all the solutions. By increasing the hydrophobicity of copolymer, the elastic response in the gel region increases

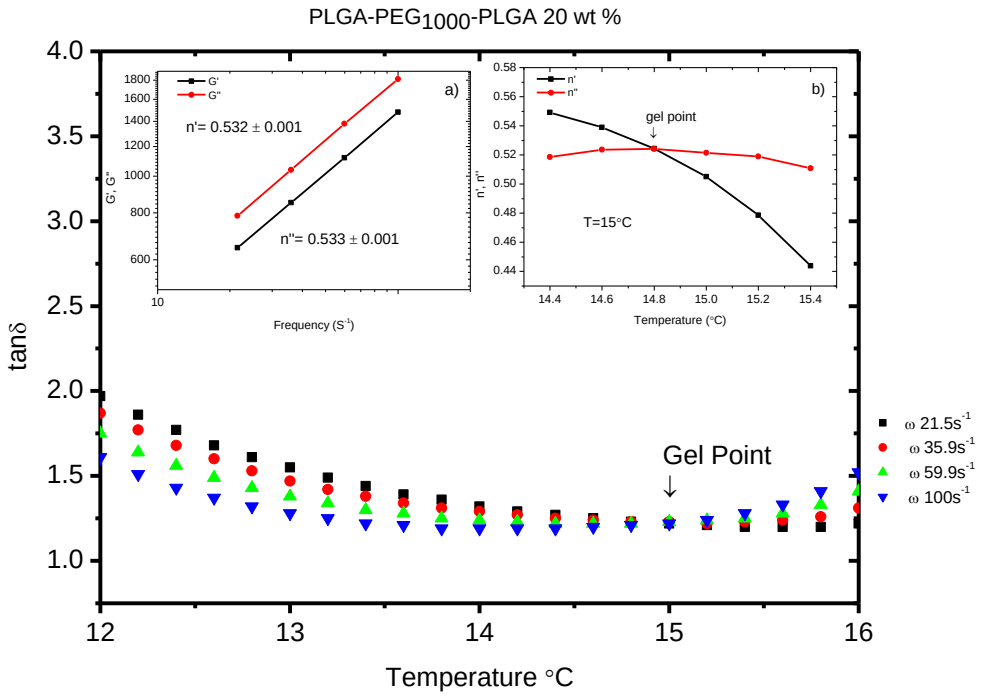

Figure 4.6 Illustration of determination of the gel point (GP) for the sample containing PLGA-PEG1000-PLGA 20 wt%. The inset a) shows frequency dependency of the storage and loss modulus for PLGA-PEG1000-PLGA 20 wt% at the gel point, showing the power law behavior. Inset b) displays the temperature dependency of n' and n'' during the gelation.

The gel point as a function of concentration of PLGA-PEG_{1000}-PLGA, PLGA-PEG_{1500}-PLGA, and their mixture is depicted in Figure 4.7 a. Solution of pure PLGA-PEG_{1000}-PLGA exhibits the lowest gel point. This can be explained by the presence of more hydrophobic interactions at high temperature in the system. Another reason that gelation occurs at higher temperature for PLGA-PEG_{1500}-PLGA compared to PLGA-PEG_{1000}-PLGA, is the formation of stable micellar structure for the copolymer with longer PEG length which is in agreement with the SANS result. Only when the temperature is very high (43°C), the contribution from the thermal energy is sufficiently high to deviate from this stable micellar structure, possibly with one of the

PLGA blocks of a chain participating in a neighboring micelle, creating an interconnected gel structure.

Figure 4.7 b shows the different ‘‘apparent’’ viscoelastic exponents plotted versus temperature. The relaxation exponents increase from 0.53 to 0.98 by increasing the concentration of PLGA-PEG_{1500}-PLGA. The phase angle δ is independent of frequency but proportional to the relaxation exponent according to eq. 5. The value of $tan\ \delta$ decreases as the relaxation exponent of the copolymer is reduced; it shows that the copolymer solutions with higher values of n, exhibit liquid-like behavior.

According to Muthukumar, when excluded-volume effects are screened out, the fractal dimension d_f can be calculated from the relaxation exponent (See section: Theoretical Models for the interpretation of n). The results suggest that the viscoelastic exponent depends on the PEG length and the value of n probably reduces with decreasing the length of PEG. The different viscoelastic exponents reflect different structures of the copolymers PLGA-PEG_{1000}-PLGA and PLGA-PEG_{1500}-PLGA at the sol–gel transition point. The fractal dimension decreases with increasing concentration of PLGA-PEG_{1500}-PLGA as it is indicated in Figure 4.7 c. It seems that the copolymer with longer PEG length forms larger lumps and more heterogeneous network than the copolymer with shorter PEG length. This probably leads to a more open network structure (lower value of fractal dimension) [76, 77].

The gel strength parameter, S, can be calculated for the incipient gels by eq. 7 [77] Figure 4.7 d presents the gel strength parameter which seems to be dependent on the PEG length in the gel network, and also, increasing the concentration of PLGA-PEG_{1000}-PLGA gives higher values of S. This suggests that increasing the concentration of copolymer with shorter PEG length gives a shorter distance between the cross-linking junctions; therefore a stronger incipient network is formed. This is probably due to formation of more stable micelles in PLGA-PEG_{1500}-PLGA system compared to PLGA-PEG_{1000}-PLGA at the same temperature

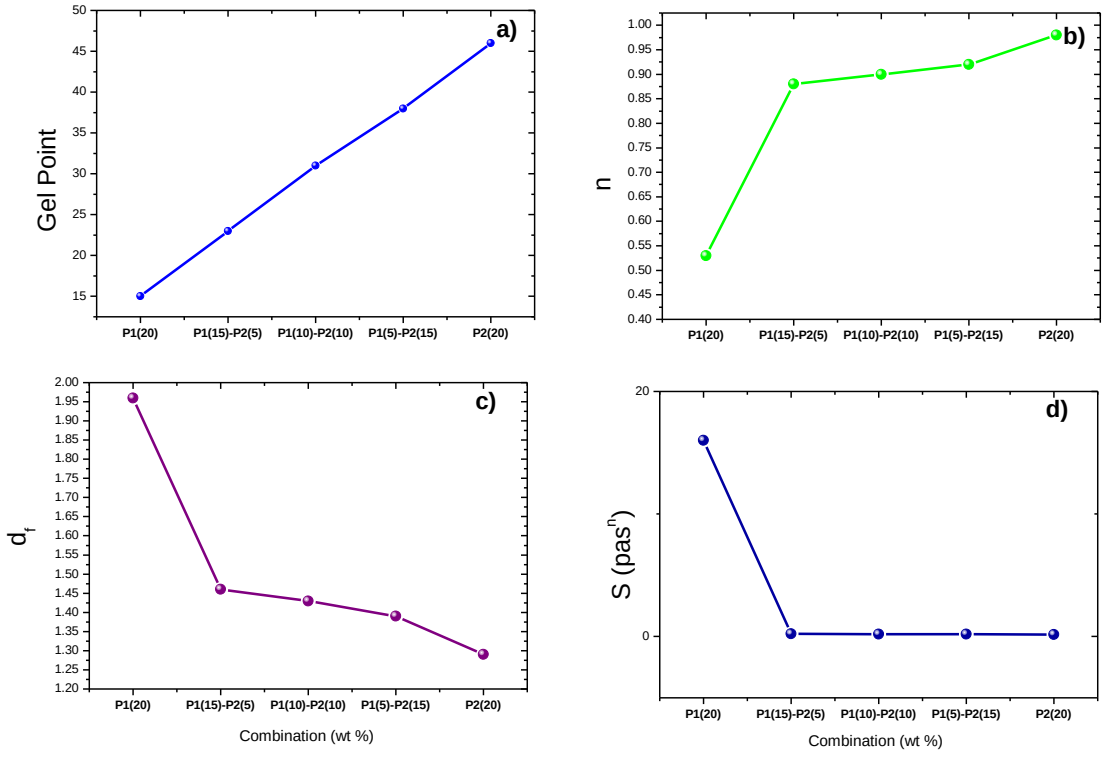

Figure 4.7 PLGA-PEG-PLGA and the combination of the two copolymer dependency of a) the gel point exponent b) the gel strength parameter c) the fractal dimension and d) the relaxation exponent (n). P1(20) = PLGA-PEG1000-PLGA 20 wt%, P1(15)+P2(5)= PLGA-PEG1000-PLGA 15 wt%+ PLGA-PEG1500-PLGA 5 wt%, P1(5)+P2(15)= PLGA-PEG1000-PLGA 5 wt%+ PLGA-PEG1500-PLGA 15 wt% and P2= PLGA-PEG1500-PLGA 20 wt%.

Table 4.1 Illustration of rheological properties (see section 2.11.3.2) of incipient gels of PLGA-PEG1000-PLGA, PLGA-PEG1500-PLGA and mixtures of the block copolymers.

Combination (wt%)	*Gel Point (G.P)*	*Fractal dimension (d_f)*	*Relaxation exponent (n)*	*Gel strength (S)*
PEG-1000 20 wt%	*15*	*1.96*	*0.53*	16
PEG-1000 15 wt% + PEG-1500 5 wt%	*23*	*1.46*	*0.88*	0.21
PEG-1000 10 wt% + PEG-1500 10 wt%	*31*	*1.43*	*0.9*	0.195
PEG-1000 5 wt% + PEG-1500 15 wt%	*38*	*1.39*	*0.92*	0.183
PEG-1500 20 wt%	*46*	*1.29*	*0.98*	0.165

4.2.4. Rheo-Small Angle Light Scattering (rheo-SALS)

Rheo-SALS is a powerful technique that allows us to simultaneously measure rheology and to acquire structural information about the sample, through the analysis of 2D-images of light scattering patterns[78]. In Figure 4.8, some 2D SALS scattered intensity patterns are shown the PLGA-PEG-PLGA solution with different PEG length at different temperatures at zero shear measurement. The scattering intensity is increasing as the temperature rises. This supports the hypothesis that larger clusters are formed as the solution approaches phase-separation.

The 2D SALS patterns for PLGA-PEG_{1000}-PLGA shows high scattering intensity at lower temperature compared to PLGA-PEG_{1500}-PLGA, because the augmented temperature-induced hydrophobicity of the polymer is more pronounced as the copolymer solution has shorter length of hydrophilic block. From the center of the Rheo-SALS images one can find, at which temperature the large associations

formed. The red color in the center of images shows the highest scattering intensity compared to yellow area. The dark circle at the center of each pattern is due to the beam stop [79].

Figure 4.8 a. indicates that scattered intensity for the PLGA-PEG_{1000}-PLGA solution is strongest at T= 23°C and 35°C. At 27°C, the intensity has dropped back to a lower value and the high intensity is observed again above 33°C. This behavior substantiate the hypothesis presented above that large interchain complexes formed at T= 23°C and 35°C.

Figure 4.8 b shows the scattered intensity is weak at low temperature and becomes more pronounced at 43°C for PLGA-PEG_{1500}-PLGA.

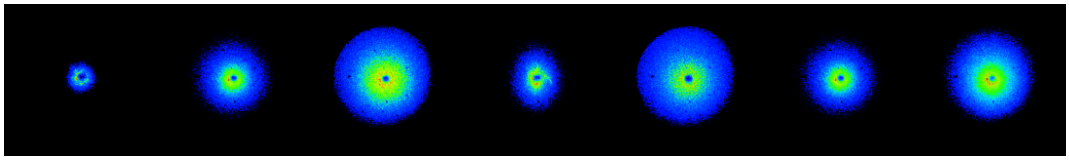

$10℃\ \gamma = 0$ $20℃\ \gamma = 0$ $23℃\ \gamma = 0$ $27℃\ \gamma = 0$ $33℃\ \gamma = 0$ $40℃\ \gamma = 0$ $50℃\ \gamma = 0$ $a)$

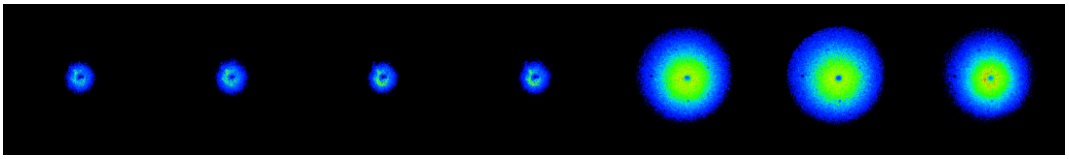

$10℃\ \gamma = 0$ $20℃\ \gamma = 0$ $30℃\ \gamma = 0$ $40℃\ \gamma = 0$ $45℃\ \gamma = 0$ $47℃\ \gamma = 0$ $50℃\ \gamma = 0$ $b)$

Figure 4.8 Effect of temperature on rheo-SALS 2D patterns for a) PLGA-PEG1000-PLGA and b)PLGA-PEG1500-PLGA 20 wt%.

A direct comparison of the rheo-SALS with the turbidity results for 20 wt% PLGA-PEG$_{1000}$-PLGA and PLGA-PEG$_{1500}$-PLGA at various temperatures is showed in Figure 4.9. The turbidity shows that large aggregates are formed at T=23°C and 33°C, while the intermicellar association is reduced at T= 10°C and 27°C for the copolymer with shorter PEG length. For the copolymer with longer PEG length, the large aggregates form at 43°C. The scattered intensities are consistent with the turbidity results at 45°C. The scattering pattern of PLGA-PEG$_{1000}$-PLGA at the temperature of 27°C is anisotropic with an elliptical scattering pattern, which suggests structural changes on this dimensional scale, that are in good agreement with the SANS result at 30°C.

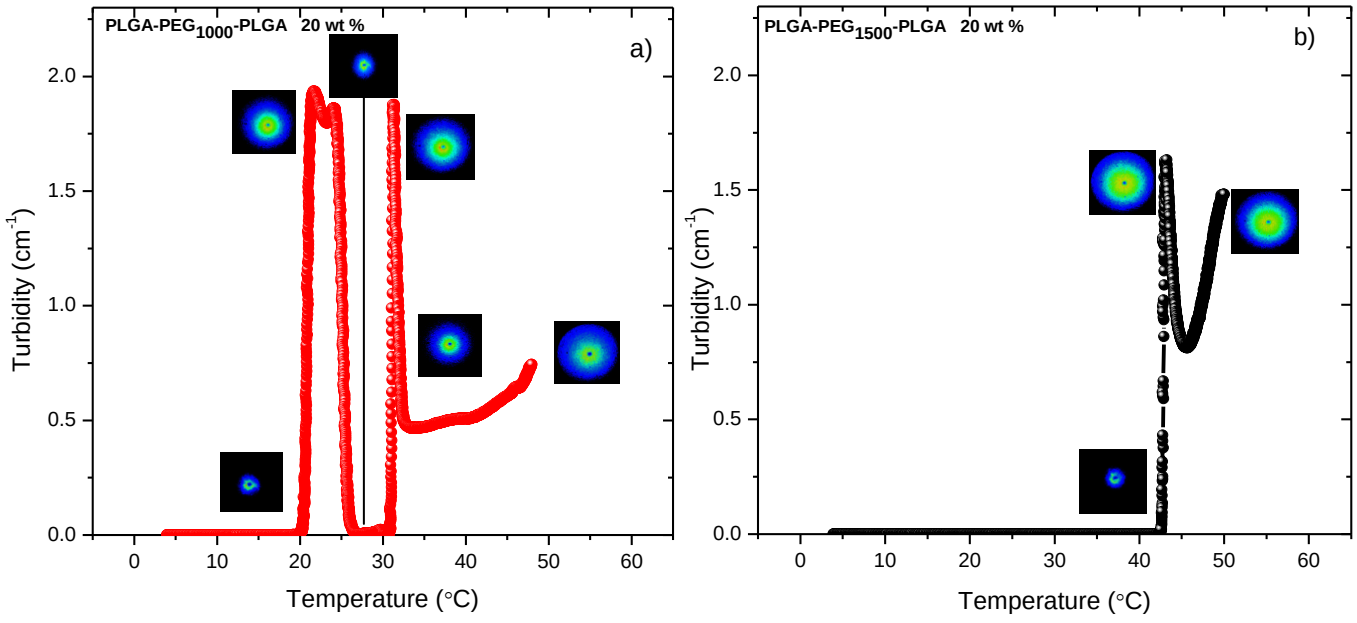

Figure 4.9 Effect of temperature on the turbidity, together with inserted rheo-SALS 2D patterns, for a) PLGA-PEG1000-PLGA and b) PLGA-PEG1500-PLGA 20 wt%.

4.2.5. Small Angle Neutron Scattering (SANS)

To study the structure of PLGA-PEG-PLGA networks on a mesoscopic dimensional scale, SANS measurement on gelling samples with different PEG length have been carried out.

The q dependencies of the scattered intensity during the gelation process for the PLGA-PEG_{1000}-PLGA, PLGA-PEG_{1500}-PLGA with a constant concentration of 20 wt% are depicted in Figure 4.10. At different temperatures, various structures of copolymers are observed. It is suggested that PLGA-PEG-PLGA forms different types of micelles at low temperature.

At temperature 10°C, the characteristic peak is observed at around q = 0.03 $Å^{-1}$ for the PLGA-PEG_{1000}-PLGA solution which shows an average micellar distance of ($q^* = 2\pi / d$), 20.9 nm. A model of core-shell micelles is used to obtain information. At temperatures below the critical gelation temperature (CGT), some bridging micelles of PLGA-PEG-PLGA copolymers formed, but they were not stable because of the low hydrophobicity of PLGA.

By increasing the temperature to the CGT (20°C), a bridged micelle network was formed because of an increase in the hydrophobicity of the PLGA segment, leading to gelation [74]. At 20°C it is observed that the correlation peak has disappeared. Thus, a cylinder model to gain information about this system is used.

As the temperature further increases (30°C), the shape changes considerably. Here a fit analysis showed that the data could be best described the rod-like micelles packed, resulting a decrease in the intermicellar interactions. The upper phase-transition of gel-to-sol at higher temperature was believed to be due to the reduction of intermicellar interactions caused by partial dehydration of the PEG blocks.

At 40°C the solution presents a new correlation peak. This peak appears at 0.04 $Å^{-1}$ that situated in higher than what it was observed at 10°C (0.03 $Å^{-1}$). The peak at 0.04 $Å^{-1}$ shows average correlation distances of 15.7 nm which is in the order of the size of a micelle, and implies a close contact in micelles. Hence, the formation of thick cylinders, consisting of several micelles packed side by side, probably tending towards a hexagonal packing of cylinders, is suggested. At 50°C, the system behaves similarly to 40°C, but with a lowering of the overall signal. We see that the correlation peak has now moved to an even higher q-value, now at ca. 0.005 nm, showing an even tighter packing of the micelles. The packing distance is now 12.5 nm. This demonstrates that the hydrophobic effect has now compressed the system even further, while keeping the number of micelles in each rod the same (low-q behavior is qualitatively the same). Note that at low temperature, this correlation distance is the intermicellar distance in the solution, whereas at 40°C and 50°C, it is the distance between tightly packed micelles.

For PLGA-PEG_{1500}-PLGA, it is important to mention that the behavior of these types of systems to be critically dependent on the length of the different blocks, thus it is likely that the difference in PEG length can explain the difference in behavior of

the PLGA-PEG_{1000}-PLGA and PLGA-PEG_{1500}-PLGA system. The copolymer with shorter PEG length presents the characteristic correlation peak around 0.03 $Å^{-1}$ at low temperature due to the interacting micelles.

This correlation peak has disappeared for PLGA-PEG_{1000}-PLGA at 20°C, i.e the transient temperature. At 30°C the pattern has changed again, showing signs of elongated (rod-like) structures. Subsequently, at 40°C, there is another drastic change, with a correlation peak appearing at 10°C, but in this case at a higher q value, showing a smaller correlation distance. At the same time, the signal increases at low q, showing the presence of large structures in the system. Finally, at 50°C, the peak has transferred to higher q values around 0.05 $Å^{-1}$, indicating an even smaller correlation distance.

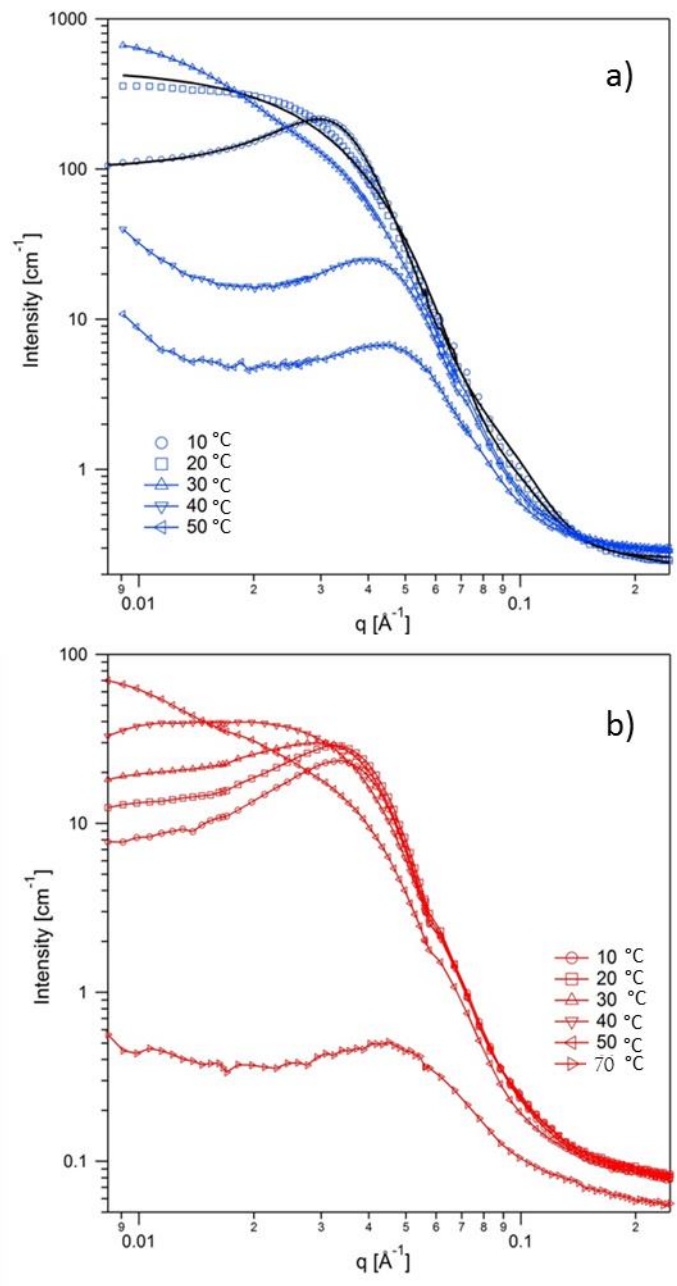

Figure 4.10 SANS scattered intensity plotted versus the scattering vector q for a) PLGA-PEG1000-PLGA 20 wt% and b) PLGA-PEG1500-PLGA 20 wt% samples at different temperatures at various stages of gelation.

The PLGA-PEG_{1500}-PLGA sample qualitatively shows the same pattern as the PLGA-PEG_{1000}-PLGA in the low and high temperature extremes. The only difference is a generally lower scattering level for the copolymer with longer PEG according to

Figure 4.11. From this, one may conclude that the two samples have similar structures below the gel point as the same as above the cloud point (50°C for PEG1000 and 70°C for PEG1500). The lower overall scattering intensity is partly due to fewer chains present in the PLGA-PEG_{1500}-PLGA micelles, since both the PLGA-PEG_{1000}-PLGA and PLGA-PEG_{1500}-PLGA solutions had the same concentration 20 wt%. The shorter average micellar distance for the solution with longer PEG length is equivalent to a larger number of particles per volume unit, and this can only occur when there are fewer chains participating in each micelle compared to the PLGA-PEG_{1000}-PLGA system. In the PLGA-PEG_{1500}-PLGA solution, the PEG chain is probably able to turn back on itself. It assembles two PLGA blocks into the same micellar core and creates a flower-like micelle. For the PLGA-PEG_{1000}-PLGA solution, the PEG chain is just too short to turn back on itself; therefore, it requires too high bending energy for the chain which is entropically unfavorable, i.e. most micelles in the PLGA-PEG_{1000}-PLGA solution have a core with only one PLGA block from each chain. The other blocks find it more energetically favorable to extend into the solution in the PLGA-PEG_{1000}-PLGA, at low temperature where the hydrophobic character of PLGA is small. The fact is that the other PLGA block for the solution stretches out in the surrounding water means that it will readily join into the core of a neighbor micelle as soon as the hydrophobic character increases slightly upon increasing the temperature. This is most likely the reason why the PLGA-PEG_{1000}-PLGA solution forms a gel at the low temperatures. While in the PLGA-PEG_{1500}-PLGA solution, the same chain has generally both its PLGA blocks located into the same micelle, which

means that the low temperature conformation (individual micelles) is more stable. Only when the temperature is very high (40°C) the contribution from the thermal energy is high enough to deviate from this stable micellar structure. This possibly happens through one of the PLGA blocks of a chain which reaches to the neighbor micelle, creating an interconnected structure (gel).

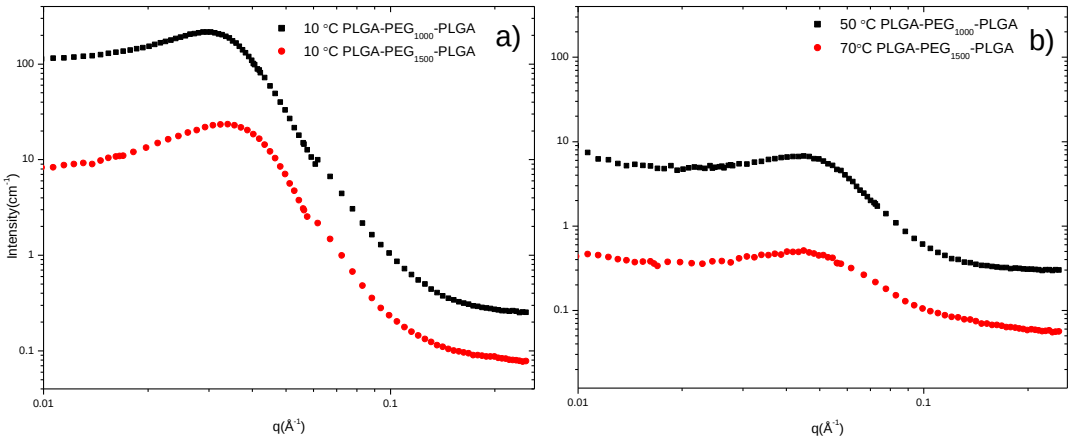

Figure 4.11 SANS scattered intensity plotted versus the scattering vector q for 20 wt% a) PLGA-PEG1500 -PLGA and b) PLGA-PEG1500-PLGA samples at different temperatures at various stages of phase separation.

According to the Figure 4.12, PLGA-PEG_{1000}-PLGA at 30°C and PLGA-PEG_{1500}-PLGA at 50°C are similar in shape. In other words, this shows that the two samples produce similar type of nanostructures in the low and high temperature but the transitions (on the nanoscale) are shifted considerably up in temperature for the sample with longer PEG length.

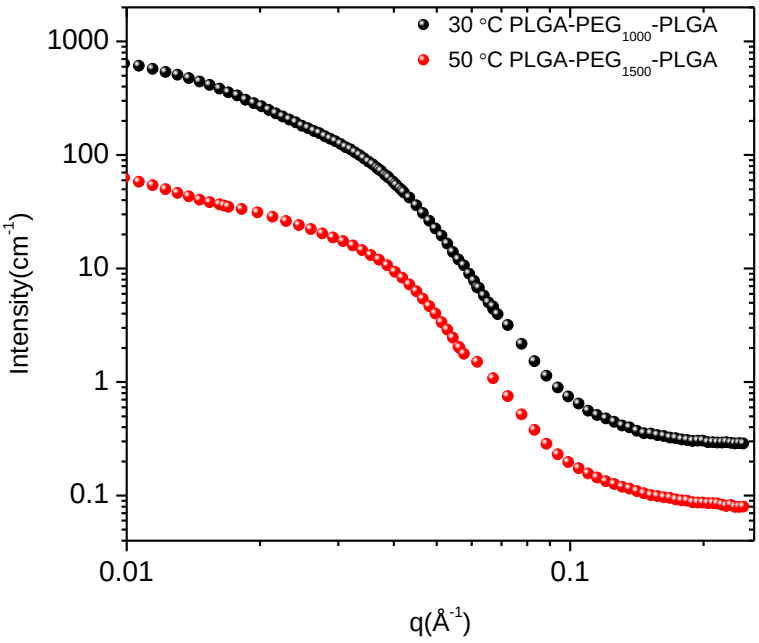

Figure 4.12 SANS scattered intensity plotted versus the scattering vector q for PLGA-PEG1500-PLGA 20 wt% and PLGA-PEG1500-PLGA 20 wt% samples at different temperatures in various stages of gelation.

5. Conclusion

In this work, some novel information about the influence of PEG length on association behavior in aqueous solutions of PLGA-PEG-PLGA has been reported. It was found that the length of PEG have a significant effect on hydrophobic association and the shape of micelles in the PLGA-PEG-PLGA solutions.

The results from turbidity have clearly demonstrated that the PEG length considerably affects the value of the cloud point for dilute aqueous solutions PLGA-PEG-PLGA. Shorter PEG chains, depress the value of the cloud point. Based on the SANS results the spherical core-shell micelles are assembled into flower-like

aggregates at different temperatures for PLGA-PEG_{1500}-PLGA. The PEG length is long enough to turn back on itself and forms these types of micelles. In contrast the PEG length in the PLGA-PEG_{1000}-PLGA is not long enough, so the PEG chains extend into solution. For copolymer with shorter PEG length, at 10°C, elongated micelles start to form and at 20°C their shape changes to an oblate like structure, and even at higher temperatures goes to disk-like shape; while the PLGA-PEG_{1500}-PLGA data shows a spherical micelle on the temperatures region from 10°C to 35°C.

The gelling behaviors of the PLGA-PEG_{1000}-PLGA and PLGA-PEG_{1500}-PLGA solutions and mixture of the copolymers with constant concentrations 20 wt% have been examined. All of the observed transition temperatures including sol-gel transition temperature (T_{gel}), the sol-precipitation transition temperature (T_{turbid}) and gel-precipitation transition temperature ($T_{precipitation}$) for the samples above CGC have been found to be decreased as PEG length increases. At the gel point, the storage and loss moduli show a power law behavior, $G \propto G'' \propto \omega^n$, with angular frequency ω. At a constant polymer concentration of 20 wt% in the semidilute regime, higher values of n are observed for pure PLGA-PEG_{1500}-PLGA and the strength of the gel is highest for pure PLGA-PEG_{1000}-PLGA. A direct comparison of the rheo-SALS with the turbidity results have been carried out for 20 wt% PLGA-PEG_{1000}-PLGA and PLGA-PEG_{1500}-PLGA at various temperatures. As the turbidity increases an increase in scattering intensity is observed. At 27°C an elliptical scattering pattern suggests structural changes on this dimensional scale, that is in good agreement with the SANS result at 30°C. The data from the SANS demonstrate several different stages

for the temperature dependence of these PLGA-PEG-PLGA copolymers. A sol state at low temperature (10°C) consisting of micelles with strong interaction, gives rise to a correlation peak indicating the intermicellar distance. The PLGA-PEG_{1000}-PLGA copolymer consists of micelles where only one of the two PLGA blocks of a chain is situated into the core, and the other extends into the solution. The length of the PEG block is sufficient for the PLGA-PEG1500-PLGA copolymer to turn back on itself, therefore both PLGA blocks can enter into the same core, creating more stable micellar structures (flower-like micelles).At 20°C for the copolymer with shorter PEG length the regular distance between micelles disappears in the sol state results in build up inter-links between the micelles in a way that a gel network is produced. But for PLGA-PEG_{1500}-PLGA this phenomenon is not observed until 40°C which originates from the better stabilized core. Subsequently at 30°C the micelles in the copolymer with shorter PEG length join into cylindrical units, most likely consisting of individual micelles aligning in one dimension. For the PLGA-PEG_{1500}-PLGA copolymer, there are only minor changes in this temperature range. These small changes are due to the effect of the enhanced thermal fluctuations. This is followed by the state of 40°C for PLGA-PEG_{1000}-PLGA, at which thick rod-like segments have been formed. These rod-like structures consist of close packed micelles, giving rise to a new correlation peak which shows short interaction distance. The same phenomenon is expected for the PLGA-PEG_{1500}-PLGA copolymer above 70°C. Finally at 50°C this overall structure is maintained for PEG with shorter length, but with an even closer packing of the micelles inside the thick rods. This most likely

takes place also for PEG with longer length at some temperature above the maximum measured temperature (70°C).

The findings from this work clearly demonstrate that the intensity of intermolecular associations would be significantly weakened when long hydrophilic chains surround the hydrophobic core. In this spirit, amphiphilic copolymers can be prepared with tunable associative properties. The results show that, for this type of copolymer, altering the length of blocks plays a prominent role in intermaicillezation.

6. Reference

1. Kjøniksen A-L, Zhu K, Pamies R and Nyström B, "Temperature-Induced Formation and Contraction of Micelle-Like Aggregates in Aqueous Solutions of Thermoresponsive Short-Chain Copolymers". *The Journal of Physical Chemistry B*, **2008**. 112(11): p. 3294-3299.

2. Liu C, Gong C, Pan Y, Zhang Y, Wang J, Huang M, Wang Y, Wang K, Gou M, Tu M, Wei Y and Qian Z, "Synthesis and Characterization of a Thermosensitive Hydrogel Based on Biodegradable Amphiphilic Pcl-Pluronic (L35)-Pcl Block Copolymers". *Colloids and Surfaces A: Physicochemical and Engineering Aspects*, **2007**. 302(1–3): p. 430-438.

3. Qiao M, Chen D, Ma X and Liu Y, "Injectable Biodegradable Temperature-Responsive Plga–Peg–Plga Copolymers: Synthesis and Effect of Copolymer Composition on the Drug Release from the Copolymer-Based Hydrogels". *International Journal of Pharmaceutics*, **2005**. 294(1–2): p. 103-112.

4. Rösler A, Vandermeulen G W M and Klok H-A, "Advanced Drug Delivery Devices Via Self-Assembly of Amphiphilic Block Copolymers". *Advanced Drug Delivery Reviews*, **2001**. 53(1): p. 95-108.

5. Chen S, Pieper R, Webster D C and Singh J, "Triblock Copolymers: Synthesis, Characterization, and Delivery of a Model Protein". *International Journal of Pharmaceutics*, **2005**. 288(2): p. 207-218.

6. Jeong J, Kim S and Park T, "Biodegradable Triblock Copolymer of Plga-Peg-Plga Enhances Gene Transfection Efficiency". *Pharmaceutical Research*, **2004**. 21(1): p. 50-54.

7. Shim W S, Yoo J S, Bae Y H and Lee D S, "Novel Injectable Ph and Temperature Sensitive Block Copolymer Hydrogel". *Biomacromolecules*, **2005**. 6(6): p. 2930-2934.

8. Veyries M L, Couarraze G, Geiger S, Agnely F, Massias L, Kunzli B, Faurisson F and Rouveix B, "Controlled Release of Vancomycin from Poloxamer 407 Gels". *International Journal of Pharmaceutics*, **1999**. 192(2): p. 183-193.

9. Zhu K, Pamies R n, Kjøniksen A-L and Nyström B, "Temperature-Induced Intermicellization of “Hairy” and “Crew-Cut” Micelles in an Aqueous Solution of a Thermoresponsive Copolymer". *Langmuir*, **2008**. 24(24): p. 14227-14233.

10. Stevens M P, "Polymer Chemistry ", *Oxford University Press,* **1999**.

11. Bates F S and Fredrickson G H, "Block Copolymer Thermodynamics: Theory and Experiment". *Annual Review of Physical Chemistry*, **1990**. 41(1): p. 525-557.

12. Lazzari M, Liu G and Lecommandoux S "Block Copolymers in Nanoscience", *John Wiley-VCH*. **2006**.

13. Hamley I W, "Developments in Block Copolymer Science and Technology", *John Wiley & Sons Ltd*, **2004**.

14. Nardin C, Widmer J, Winterhalter M and Meier W, "Amphiphilic Block Copolymer Nanocontainers as Bioreactors". *The European Physical Journal E*, **2001**. 4(4): p. 403-410.

15. Rodríguez-Hernández J, Chécot F, Gnanou Y and Lecommandoux S, "Toward 'Smart' Nano-Objects by Self-Assembly of Block Copolymers in Solution". *Progress in Polymer Science*, **2005**. 30(7): p. 691-724.

16. Paschalis Alexandridis B L, "Amphiphilic Block Copolymers: Self-Assembly and Applications". **2000**, Elsevier Science.

17. Pispas S, Hadjichristidis N, Potemkin I and Khokhlov A, "Effect of Architecture on the Micellization Properties of Block Copolymers: A2b Miktoarm Stars Vs Ab Diblocks". *Macromolecules*, **2000**. 33(5): p. 1741-1746.

18. Riess G, "Micellization of Block Copolymers". *Progress in Polymer Science*, **2003**. 28(7): p. 1107-1170.

19. Förster S and Antonietti M, "Amphiphilic Block Copolymers in Structure-Controlled Nanomaterial Hybrids". *Advanced Materials*, **1998**. 10(3): p. 195-217.

20. Xia Y-q, Guo T-y, Song M-d, Zhang B-h and Zhang B-l, "Hemoglobin Recognition by Imprinting in Semi-Interpenetrating Polymer Network Hydrogel Based on Polyacrylamide and Chitosan". *Biomacromolecules*, **2005**. 6(5): p. 2601-2606.

21. Cong J, Zhang X, Chen K and Xu J, "Fiber Optic Bragg Grating Sensor Based on Hydrogels for Measuring Salinity". *Sensors and Actuators B: Chemical*, **2002**. 87(3): p. 487-490.

22. Hoffman A S, "Hydrogels for Biomedical Applications". *Advanced Drug Delivery Reviews*, **2002**. 54(1): p. 3-12.

23. Song J Y, Wang Y Y and Wan C C, "Review of Gel-Type Polymer Electrolytes for Lithium-Ion Batteries". *Journal of Power Sources*, **1999**. 77(2): p. 183-197.

24. Yu L and Ding J, "Injectable Hydrogels as Unique Biomedical Materials". *Chemical Society Reviews*, **2008**. 37(8): p. 1473-1481.

25. Qiu Y and Park K, "Environment-Sensitive Hydrogels for Drug Delivery". *Advanced Drug Delivery Reviews*, **2001**. 53(3): p. 321-339.

26. Jeong B, Lee D S, Shon J-I, Bae Y H and Kim S W, "Thermoreversible Gelation of Poly(Ethylene Oxide) Biodegradable Polyester Block Copolymers". *Journal of Polymer Science Part A: Polymer Chemistry*, **1999**. 37(6): p. 751-760.

27. Shim W S, Kim S W and Lee D S, "Sulfonamide-Based Ph- and Temperature-Sensitive Biodegradable Block Copolymer Hydrogels". *Biomacromolecules*, **2006**. 7(6): p. 1935-1941.

28. Skrabania K, Kristen J, Laschewsky A, Akdemir Ö, Hoth A and Lutz J-F, "Design, Synthesis, and Aqueous Aggregation Behavior of Nonionic Single and Multiple Thermoresponsive Polymers†". *Langmuir*, **2006**. 23(1): p. 84-93.

29. David Samuel Simmons B S, "Phase and Conformational Behavior of Lcst-Driven Stimuli Responsive Polymers". *Thesis*, **2009**.

30. Fariba Ganji E V-F, "Hydrogels in Controlled Drug Delivery Systems". *Iranian Polymer Journal*, **2009**. 18(63): p. 88.

31. Geever L, Nugent M D and Higginbotham C, "The Effect of Salts and Ph Buffered Solutions on the Phase Transition Temperature and Swelling of Thermoresponsive Pseudogels Based on N-Isopropylacrylamide". *Journal of Materials Science*, **2007**. 42(23): p. 9845-9854.

32. Zhang L P, Noda I and Wu Y, "An Application of Concatenated 2d Correlation Spectroscopy: Exploration of the Reversibility of the Temperature-Induced Hydration Variation of Poly(N-Isopropylmethacrylamide) in Aqueous Solution". *Journal of Molecular Structure*, **2010**. 974(1–3): p. 80-87.

33. Vermonden T, Jena S S, Barriet D, Censi R, van der Gucht J, Hennink W E and Siegel R A, "Macromolecular Diffusion in Self-Assembling Biodegradable Thermosensitive Hydrogels". *Macromolecules*, **2009**. 43(2): p. 782-789.

34. Jeong B, Kim S W and Bae Y H, "Thermosensitive Sol–Gel Reversible Hydrogels". *Advanced Drug Delivery Reviews*, **2002**. 54(1): p. 37-51.

35. Jeong B, Bae Y H and Kim S W, "Thermoreversible Gelation of Peg−Plga−Peg Triblock Copolymer Aqueous Solutions". *Macromolecules*, **1999**. 32(21): p. 7064-7069.

36. Hadjichristidis N, Pitsikalis M and Iatrou H, "Synthesis of Block Copolymers", in *Block Copolymers I*. V. Abetz, Editor. **2005**, Springer Berlin Heidelberg. p. 1-124.

37. Adams M L, Lavasanifar A and Kwon G S, "Amphiphilic Block Copolymers for Drug Delivery". *Journal of Pharmaceutical Sciences*, **2003**. 92(7): p. 1343-1355.

38. Jain R A, "The Manufacturing Techniques of Various Drug Loaded Biodegradable Poly(Lactide-Co-Glycolide) (Plga) Devices". *Biomaterials*, **2000**. 21(23): p. 2475-2490.

39. Menemşe KİREMİTÇİ-GÜMÜŞDERELİOĞLU G D, "Synthesis, Characterization and in Vitro Degradation of Poly(Dl-Lactide)/Poly(Dl-Lactide-Co-Glycolide) Films". *Turkish Journal of Chemistry*, **1999**. 23(153): p. 162.

40. Astete C E and Sabliov C M, "Synthesis and Characterization of Plga Nanoparticles". *Journal of Biomaterials Science, Polymer Edition*, **2006**. 17(3): p. 247-289.

41. Lü J-M, Wang X, Marin-Muller C, Wang H, Lin P H, Yao Q and Chen C, "Current Advances in Research and Clinical Applications of Plga-Based Nanotechnology". *Expert Review of Molecular Diagnostics*, **2009**. 9(4): p. 325-341.

42. Kumari A, Yadav S K and Yadav S C, "Biodegradable Polymeric Nanoparticles Based Drug Delivery Systems". *Colloids and Surfaces B: Biointerfaces*, **2010**. 75(1): p. 1-18.

43. French A C, Thompson A L and Davis B G, "High-Purity Discrete Peg-Oligomer Crystals Allow Structural Insight". *Angewandte Chemie*, **2009**. 121(7): p. 1274-1278.

44. Delgado C, Francis G E and Fisher D, "The Uses and Properties of Peg-Linked Proteins". *Critical reviews in therapeutic drug carrier systems*, **1992**. 9(3-4): p. 249-304.

45. Yu L, Zhang H and Ding J, "A Subtle End-Group Effect on Macroscopic Physical Gelation of Triblock Copolymer Aqueous Solutions". *Angewandte Chemie International Edition*, **2006**. 45(14): p. 2232-2235.

46. Song Z, Feng R, Sun M, Guo C, Gao Y, Li L and Zhai G, "Curcumin-Loaded Plga-Peg-Plga Triblock Copolymeric Micelles: Preparation, Pharmacokinetics and Distribution in Vivo". *Journal of Colloid and Interface Science*, **2011**. 354(1): p. 116-123.

47. Ghahremankhani A A, Dorkoosh F and Dinarvand R, "Plga-Peg-Plga Tri-Block Copolymers as in Situ Gel-Forming Peptide Delivery System: Effect of Formulation Properties on Peptide Release". *Pharmaceutical Development and Technology*, **2008**. 13(1): p. 49-55.

48. Fujiwara T, Yamaoka T and Kimura Y, "Thermo-Responsive Biodegradable Hydrogels from Stereocomplexed Poly(Lactide)S", in *Biomedical Applications of Hydrogels Handbook*. R.M. Ottenbrite, K. Park and T. Okano, Editors. **2010**, Springer New York. p. 157-177.

49. Lee Y, Chung H J, Yeo S, Ahn C-H, Lee H, Messersmith P B and Park T G, "Thermo-Sensitive, Injectable, and Tissue Adhesive Sol-Gel Transition Hyaluronic Acid/Pluronic Composite Hydrogels Prepared from Bio-Inspired Catechol-Thiol Reaction". *Soft Matter*, **2010**. 6(5): p. 977-983.

50. Singh S, Webster D C and Singh J, "Thermosensitive Polymers: Synthesis, Characterization, and Delivery of Proteins". *International Journal of Pharmaceutics*, **2007**. 341(1–2): p. 68-77.

51. Jeong B, Han Bae Y and Wan Kim S, "Biodegradable Thermosensitive Micelles of Peg-Plga-Peg Triblock Copolymers". *Colloids and Surfaces B: Biointerfaces*, **1999**. 16(1–4): p. 185-193.

52. Soga O, van Nostrum C F, Ramzi A, Visser T, Soulimani F, Frederik P M, Bomans P H H and Hennink W E, "Physicochemical Characterization of Degradable Thermosensitive Polymeric Micelles". *Langmuir*, **2004**. 20(21): p. 9388-9395.

53. Vermonden T, Besseling N A M, van Steenbergen M J and Hennink W E, "Rheological Studies of Thermosensitive Triblock Copolymer Hydrogels". *Langmuir*, **2006**. 22(24): p. 10180-10184.

54. Tang Y, Oak M, Mandke R, Layek B, Sharma G and Singh J, "Thermosensitive Polymers for Controlled Delivery of Hormones", in *Active Implants and Scaffolds for Tissue Regeneration*. M. Zilberman, Editor. **2011**, Springer Berlin Heidelberg. p. 457-479.

55. Jeong B, Lee K M, Gutowska A and An Y H, "%Thermogelling Biodegradable Copolymer Aqueous Solutions for Injectable Protein Delivery and Tissue Engineering". *Biomacromolecules*, **2002**. 3(4): p. 865-868.

56. Calejo M T, Cardoso A M S, Kjøniksen A-L, Zhu K, Morais C M, Sande S A, Cardoso A L, Lima M C P d, Jurado A and Nyström B, "Temperature-Responsive Cationic Block Copolymers as Nanocarriers for Gene Delivery". *International Journal of Pharmaceutics*, **2013**. 448(1): p. 105-114.

57. Ayoubi M A, Zhu K, Nystrom B, Almdal K, Olsson U and Piculell L, "Micro- and Nanophase Separations in Hierarchical Self-Assembly of Strongly Amphiphilic Block Copolymer-Based Ionic Supramolecules". *Soft Matter*, **2013**. 9(5): p. 1540-1555.

58. Behrens M A, Kjøniksen A-L, Zhu K, Nyström B and Pedersen J S, "Small-Angle X-Ray Scattering Study of Charged Triblock Copolymers as a Function of Polymer Concentration, Temperature, and Charge Screening". *Macromolecules*, **2011**. 45(1): p. 246-255.

59. Maleki A, Kjøniksen A-L, Knudsen K D and Nyström B, "Dynamical and Structural Behavior of Hydroxyethylcellulose Hydrogels Obtained by Chemical Gelation". *Polymer International*, **2006**. 55(3): p. 365-374.

60. Chung Y-M, Simmons K L, Gutowska A and Jeong B, "Sol−Gel Transition Temperature of Plga-G-Peg Aqueous Solutions". *Biomacromolecules*, **2002**. 3(3): p. 511-516.

61. Yao A, Tassieri M, Padgett M and Cooper J, "Microrheology with Optical Tweezers". *Lab on a Chip*, **2009**. 9(17): p. 2568-2575.

62. Silioc C, Maleki A, Zhu K, Kjøniksen A-L and Nyström B, "Effect of Hydrophobic Modification on Rheological and Swelling Features During Chemical Gelation of Aqueous Polysaccharides". *Biomacromolecules*, **2007**. 8(2): p. 719-728.

63. Bu H, Kjøniksen A-L and Nyström B, "Effects of Ph on Dynamics and Rheology During Association and Gelation Via the Ugi Reaction of Aqueous Alginate". *European Polymer Journal*, **2005**. 41(8): p. 1708-1717.

64. Nyström B, Kjøniksen A-L and Lindman B, "Effects of Temperature, Surfactant, and Salt on the Rheological Behavior in Semidilute Aqueous Systems of a Nonionic Cellulose Ether". *Langmuir*, **1996**. 12(13): p. 3233-3240.

65. Zhu K, Jin H, Kjøniksen A-L and Nyström B, "Anomalous Transition in Aqueous Solutions of a Thermoresponsive Amphiphilic Diblock Copolymer". *The Journal of Physical Chemistry B*, **2007**. 111(37): p. 10862-10870.

66. Guinier A and Fournet G, "Small-Angle Scattering of X-Rays". John Wiley & Sons Ltd, **1955**.

67. Bu H, Kjøniksen A-L, Knudsen K D and Nyström B, "Effects of Surfactant and Temperature on Rheological and Structural Properties of Semidilute Aqueous Solutions of Unmodified and Hydrophobically Modified Alginate". *Langmuir*, **2005**. 21(24): p. 10923-10930.

68. Wu J, Wei W, Wang L-Y, Su Z-G and Ma G-H, "A Thermosensitive Hydrogel Based on Quaternized Chitosan and Poly(Ethylene Glycol) for Nasal Drug Delivery System". *Biomaterials*, **2007**. 28(13): p. 2220-2232.

69. Bu H, Kjøniksen A-L, Knudsen K D and Nyström B, "Characterization of Interactions in Aqueous Mixtures of Hydrophobically Modified Alginate and Different Types of Surfactant". *Colloids and Surfaces A: Physicochemical and Engineering Aspects*, **2007**. 293(1–3): p. 105-113.

70. Pamies R, Zhu K, Kjøniksen A-L, Knudsen K D and Nyström B, "Temperature-Induced Intermicellization and Contraction in Aqueous Mixtures of Sodium Dodecyl Sulfate and an Amphiphilic Diblock Copolymer". *Journal of Colloid and Interface Science*, **2008**. 326(1): p. 76-88.

71. Kjøniksen A-L, Galant C, Knudsen K D, Nguyen G T M and Nyström B, "Effects of B-Cyclodextrin Addition and Temperature on the Modulation of Hydrophobic Interactions in Aqueous Solutions of an Associative Alginate". *Biomacromolecules*, **2005**. 6(6): p. 3129-3136.
72. Lee D and He C, "In-Situ Gelling Stimuli-Sensitive Peg-Based Amphiphilic Copolymer Hydrogels", in *Biomedical Applications of Hydrogels Handbook*. R.M. Ottenbrite, K. Park and T. Okano, Editors. **2010**, Springer New York. p. 123-146.

73. Eugene Lih Y K J, Jin Woo Bae, Ki Dong Park, "An in Situ Gel-Forming Heparin-Conjugated Plga-Peg-Plga Copolymer". *Bioactive and Compatible Polymers September*, **2008**. 23(443): p. 749.
74. Nguyen M K and Lee D S, "Injectable Biodegradable Hydrogels". *Macromolecular Bioscience*, **2010**. 10(6): p. 563-579.

75. Pamies R, Zhu K, Kjøniksen A-L and Nyström B, "Thermal Response of Low Molecular Weight Poly-(N-Isopropylacrylamide) Polymers in Aqueous Solution". *Polymer Bulletin*, **2009**. 62(4): p. 487-502.

76. Kjøniksen A-L and Nyström B, "Effects of Polymer Concentration and Cross-Linking Density on Rheology of Chemically Cross-Linked Poly(Vinyl Alcohol) near the Gelation Threshold". *Macromolecules*, **1996**. 29(15): p. 5215-5222.

77. Calejo M T, Kjøniksen A-L, Pinazo A, Pérez L, Cardoso A M S, Pedroso de Lima M C, Jurado A S, Sande S A and Nyström B, "Thermoresponsive Hydrogels with Low Toxicity from Mixtures of Ethyl(Hydroxyethyl) Cellulose and Arginine-Based Surfactants". *International Journal of Pharmaceutics*, **2012**. 436(1–2): p. 454-462.

78. Calejo M T, Kjøniksen A-L, Marques E F, Araújo M J, Sande S A and Nyström B, "Interactions between Ethyl(Hydroxyethyl) Cellulose and Lysine-Based Surfactants in Aqueous Media". *European Polymer Journal*, **2012**. 48(9): p. 1622-1631.

79. Pamies R n, Zhu K, Volden S, Kjøniksen A-L, Karlsson G r, Glomm W R and Nyström B, "Temperature-Induced Flocculation of Gold Particles with an Adsorbed Thermoresponsive Cationic Copolymer". *The Journal of Physical Chemistry C*, **2010**. 114(50): p. 21960-21968.